Trabajo Fin de Grado

Grado en Ingeniería Civil

“Characterization of the dynamic damping properties of a fiber-reinforced metaconcrete”

Autora: Violeta González Villegas

Tutor: Héctor Cifuentes Bulté

Miguel Molinos Pérez

Dpto. de Mecánica de Medios Continuos y Teoría de Estructuras

Escuela Técnica Superior de Ingeniería

Sevilla, 2024

Trabajo Fin de Grado
Grado en Ingeniería Civil

“Characterization of the dynamic damping properties of a fiber-reinforced metaconcrete”

Autora:
Violeta González Villegas

Tutor:
Héctor Cifuentes Bulté
Catedrático de Universidad
Miguel Molinos Pérez
Contrato Juan de la Cierva Formación

Dpto. de Mecánica de Medios Continuos y Teoría de Estructuras
Escuela Técnica Superior de Ingeniería
Universidad de Sevilla
Sevilla, 2024

Trabajo Fin de Grado: “Characterization of the dynamic damping properties of a fiber-reinforced metaconcrete”

Autora: Violeta González Villegas

Tutor: Héctor Cifuentes Bulté

Miguel Molinos Pérez

El tribunal nombrado para juzgar el Proyecto arriba indicado, compuesto por los siguientes miembros:

Presidente:

Vocales:

Secretario:

Acuerdan otorgarle la calificación de:

Sevilla, 2024

El Secretario del Tribunal

Agradecimientos

A mi familia, por haberme permitido seguir haciendo lo que más valoro en este mundo, formarme y enriquecer mi saber. A mi madre, por haber sido mi mayor apoyo y ayuda, y haber estado ahí cuando más falta me hacía sacrificándose siempre por mí. A mi hermano, por haber sido mi modelo a seguir y preocuparse porque no hiciera más de lo que podía. A mi padre, por haber hecho esos momentos duros menos pesados con sus bromas y sus palabras de ánimos. A mi abuela, por ser la que más se ilusiona con mis aprobados, por verse todos los programas de ingeniería que salen en la tele, porque "quién le iba a decir a ella que iba a tener una nieta *Ingeniera de Caminos*".

A Pedro, por haberme ayudado siempre con todo lo que podía y haberme dado fuerza cuando la necesitaba.

A mi tutor Héctor, por confiar en mí y por impartirme *Estructuras de Hormigón I* tan admirablemente que me hizo decantarme por la que ahora es mi especialidad.

Violeta González Villegas

Sevilla, 2024

Resumen

Este trabajo se centra en la caracterización de las propiedades dinámicas de amortiguación de un material reforzado con distintos tipos de fibras llamado metahormigón. Los metahormigones son un tipo de metamaterial diseñado para tener propiedades específicas que no se encuentran en los materiales convencionales. Estas propiedades se logran mediante la agregación de fibras que controlan la propagación de ondas, y en consecuencia, amortiguan las vibraciones producidas en el hormigón. El objetivo de este Trabajo Fin de Grado es la validación experimental de las propiedades amortiguadoras de varios especímenes de metahormigón reforzado con distintos tipos de fibras sometidos a ondas de alta frecuencia.

Para la campaña experimental se utilizaron 4 tipos distintos de especímenes de metahormigón de ultra alta resistencia reforzado con diferentes fibras: un hormigón convencional sin fibras (D0), un metahormigón reforzado con fibras cortas (DS), un metahormigón reforzado con fibras largas (DL) y un metahormigón híbrido reforzado con una proporción 50/50 de fibras cortas y largas (DSL). De cada tipo de espécimen se sacaron a su vez 4 probetas cúbicas para poder promediar las medidas registradas. De esta forma, las 16 probetas fueron sometidas a un rango de frecuencias de 0 Hz hasta 25,000 Hz generadas por un altavoz colocado en la cara superior de la probeta. A su vez, se recogieron datos de aceleraciones con 2 acelerómetros, uno en la cara superior de la probeta (RW) y otro en la cara inferior (DW).

Las aceleraciones recogidas se pasaron al dominio de la frecuencia a través de la Transformada Rápida de Fourier (FFT) para su análisis, obteniendo la respuesta promediada de todos los especímenes para cada frecuencia. Los resultados de las aceleraciones en el dominio de la frecuencia muestran un comportamiento amortiguador de los metahormigones para un cierto rango de frecuencias, obteniendo para otros rangos un comportamiento contrario.

Para obtener una mejor discusión de los resultados se hizo uso de un parámetro denominado transmisibilidad, el cual cuantifica la disminución de aceleraciones en comparación con otra de referencia. En este caso se ha estudiado las transmisibilidades de los metahormigones (DS, DL y DSL) con respecto al espécimen convencional sin fibras (D0).

Los resultados obtenidos muestran para ciertos rangos de frecuencias una clara atenuación de las vibraciones registradas, cumpliendo así la hipótesis contemplada. Para otros rangos su análisis es un poco más complejo y se observan aumentos de las aceleraciones registradas.

De esta forma, con este trabajo se contribuye a la compresión de las capacidades de amortiguación de los metahormigones de ultra alta resistencia reforzados con fibras y su potencial para mejorar la resistencia de las estructuras frente a cargas dinámicas, lo cual resulta de gran relevancia para aplicaciones en la Ingeniería Civil donde la reducción de vibraciones es crucial.

Abstract

This project focuses on studying the damping properties of a material called metaconcrete, which is reinforced with different types of fibers. Metaconcretes are special materials designed to have unique properties not found in regular concrete. These properties are achieved by adding fibers that control wave propagation and reduce vibrations in the concrete. The goal of this project is to experimentally validate the damping properties of various fiber-reinforced metaconcrete specimens subjected to high-frequency waves.

For the experimental campaign, 4 types of ultra-high-strength metaconcrete specimens reinforced with different fibers were used: conventional concrete without fibers (D0), metaconcrete with short fibers (DS), metaconcrete with long fibers (DL), and hybrid metaconcrete with a 50/50 mix of short and long fibers (DSL). Four cubic samples were taken from each type of specimen to average the measurements. The 16 samples were exposed to frequencies ranging from 0 Hz to 25,000 Hz using a speaker placed on the top surface of the cube. Acceleration data were collected using 2 accelerometers, one on the top surface (RW) and one on the bottom surface (DW).

The collected acceleration data were transformed into the frequency domain using the Fast Fourier Transform (FFT) for analysis. The results showed that metaconcretes have damping properties within certain frequency ranges, while exhibiting the opposite behavior in other ranges.

For a better discuss of the results, a parameter called transmissibility was used, which measures the reduction of accelerations compared to another acceleration of reference. In this study, the transmissibilities of the metaconcretes (DS, DL, and DSL) were compared to the conventional concrete without fibers (D0).

The results showed a clear reduction in vibrations within certain frequency ranges, confirming the hypothesis. For other ranges, the analysis was more complex and increases in the recorded accelerations are observed.

This project helps to understand the damping capabilities of ultra-high-strength fiber-reinforced metaconcretes and their potential to improve the resistance of structures against dynamic loads. This is important for Civil Engineering applications where reducing vibrations is crucial.

Index

FIGURE INDEX

TABLE INDEX

1 INTRODUCTION

In the past few years, researchers have started studying artificial composite materials with enhanced properties. These materials, known as metamaterials, have potential uses in various engineering applications. This project explores metaconcrete, a metamaterial made of ultra-high-strength concrete with steel fiber inclusions. In this chapter, the current state of the art is discussed, the objectives are outlined, and a summary of the content is provided.

1.1 Motivation

Metamaterials are innovative materials whose properties depend on both the properties of their constituent materials and their engineered microstructure, based on simple mechanical models.

These metamaterials can be designed to control the effect of external forces on systems that exhibit wave diffusion. They take advantage of unusual properties such as a negative refractive index, negative shear modulus, or negative effective mass [1]. These properties are achieved by introducing specially designed and arranged inclusions, which help recreate and control desired behaviors when the composite interacts with waves.

Initially, metamaterials were developed to control the propagation of electromagnetic waves and manipulate fields visible to the human eye. However, their study has expanded to various engineering fields, leading to numerous investigations into applying the same concepts to waves of different frequencies.

One example of metamaterials is metaconcrete, which consists of a cementitious matrix with aggregates of different nature. Studies and experimental validations have been conducted using spherical bi-material inclusions, with one particular study serving as a reference for continued research.

This thesis experimentally verifies the attenuation capabilities of metaconcrete under sonic field stresses. An experimental campaign was conducted on cylindrical specimens with arranged heterogeneous inclusions. The results show that attenuation occurs at frequencies close to the resonance frequencies of the inclusions [2].

This leads to the possibility of studying the damping capacity of different metaconcretes with different inclusions, like fiber-reinforced concrete. This type of concrete is already used in Civil Engineering and offers advantages over regular concrete.

1.2 Objectives of the study

This study aims to enhance the understanding of the attenuation properties of fibers in metaconcrete by using ultra-high-strength concrete with various types of fiber reinforcement. Two types of fibers will be tested to evaluate their effects and achieve more conclusive results.

To conduct the experiment, the specimens will be excited across a wide range of frequencies to induce resonance in the fibers. Ultrasound from a speaker will be used to excite the specimens, and accelerations will be measured on both faces of the cube. The data will be analyzed in the frequency domain using a Fast Fourier Transform (FFT) made with Dewesoft software.

The objective is to verify if the accelerations recorded in the specimens with fibers decrease compared to a specimen without any inclusions. To achieve this, a parameter called transmissibility will be used, which relates these accelerations from the FFTs. This parameter is obtained by applying a similar method to other used by researchers for photonic and acoustic crystals [3].

1.3 Project structure

This project is organized as follows:

- Chapter 1 introduces metamaterials and metaconccrete, discussing briefly the state of the art and the objectives of this project.
- Chapter 2 provides a more complete review of existing literature in metamaterials and metaconcrete, focusing on their properties and applications.
- Chapter 3 describes the specimens used, the experimental setup, and the experimental and data processing procedures.
- Chapter 4 presents the results from the wave transmission tests and analyzes the dynamic behavior of the specimens.
- Chapter 5 discusses the results of the experimental analysis.
- Chapter 6 offers conclusions on the effectiveness of fiber-reinforced metaconcrete and suggests potential directions for future research based on the study's results and conclusions.
- Appendix includes additional information on frequency sweeps, FFT averages, and transmissibility data.

2 BACKGROUND

In this chapter, existing literature and studies related to this new type of materials, specifically metaconcrete, are examined. To continue the line of research, a comprehensive literature review has been conducted to establish the current state of knowledge. The following essential studies have been used as references:

- Several articles on metamaterials and metaconcrete, covering investigations into elastic wave transmission and its mitigation properties.
- A master's thesis exploring metaconcrete reinforce with bi-material inclusions.

2.1 Metamaterials

As discussed in *section 1.1* of *Chapter 1*, "*Introduction*", there have been significant advancements in designing metamaterials engineered to demonstrate unconventional properties. These complex composites derive their unique characteristics from carefully designed microstructures [4].

Early studies began exploring the use of metamaterials to manipulate electromagnetic waves, influencing the development of sonic and phononic crystals, which are the acoustic counterparts of photonic crystals. Basic phononic crystals, consisting of periodic arrays of cylinders, have demonstrated effective wave filtering capabilities [5], [6].

These crystals enable the creation of frequency bands where incident energy disperses or scatters, leading to partial or complete absorption of elastic waves propagating through the medium and subsequently reducing the waves detected exiting the body. Such materials often use the periodic arrangement of their internal structure to create Bragg-type bandgaps [7]. For instance, an investigation into sound attenuation by a sculpture in Madrid was introduced and formally presented with experimental analysis a few years later [8].

This led to the development of a new composite material consisting of an inner sphere made of high-density material (lead) coated with a soft material (silicone), immersed in an epoxy matrix. As sonic waves pass through the material, resonance of the heavy core can be activated at selected frequencies, resulting in resonance-induced band gaps [9].

Materials incorporating resonant inclusions exhibit wave attenuation properties due to their unique characteristics, such as negative effective mass. Normally, mass density is defined as the volume average of constituent masses. However, during dynamic excitation with resonant inclusions, relative motion between the constituents and the matrix alters the dynamic effective mass density compared to its static counterpart [10], [11]. This modification can lead to a significantly large and negative effective mass when the resonance of the heavy internal mass is activated, allowing these structures to effectively manipulate and reduce wave energy. Metaconcrete, recently introduced by Mitchell et al. [4], illustrates this concept.

2.2 Metaconcrete

Metaconcrete is introduced as a modified concrete designed to reduce damage and energy propagation caused by dynamic loading, such as blast loading from explosions. Traditional aggregates in concrete are replaced with bi-material inclusions that alter the dynamic response of the system across typical frequency spectra for rapid dynamic actions [4]. These new aggregates consist of spherical inclusions with a heavy metal core coated with a layer of soft material, possibly enclosed within a thin steel protective shell. At specific frequencies, these aggregates exhibit resonant behavior, oscillating around their equilibrium position and thereby absorbing a portion of the mechanical energy supplied to the system.

The beneficial energy transfer and the implications of resonance-induced negative effective mass highlight the importance of studying metaconcrete cubes under fixed frequencies of applied loading. Transmission ratio plots, commonly used to evaluate bandgaps and resonance-induced behaviors in phononic crystals with similar layered structures [3], can also be applied to metaconcrete. These plots evaluate the change in wave amplitude across a material in relation to input wave frequency. Analyzing these ratios for metaconcrete provides insights into its transmission characteristics and the activation of resonance at various excitation frequencies. This method enables a more precise determination of aggregate properties suited for specific loading applications.

Several experimental validations have been conducted. In a 2017 article, a non-destructive dynamic test was performed on metaconcrete specimens using a wide range of ultrasound frequencies [1]. The transmitted amplitude through the cube was measured, revealing a reduction of two orders of magnitude compared to conventional concrete. Additionally, a subsequent thesis extended this research [2], conducting a more detailed study and confirming the effective mitigation of transmitted waves. These experiments lay the groundwork for future research, as experimental validation of other types of metaconcrete is still unavailable.

Figure 2.1: inclusions used in the thesis "Metaconcrete: Experimental Investigation on Samples with Inhomogeneous Inclusions" [2]

This study provides an initial experimental validation of the attenuating properties of ultra-high-strength fiber-reinforced metaconcrete. The research is motivated by the recent integration of metamaterials in civil engineering, specifically in dynamics and elastic wave transmission. Our objective is to assess the practical functionality of using this concrete, which has already found application in this field, to determine its competitiveness compared to traditional construction materials.

2.3 Application in Civil Engineering

The possibility of achieving attenuations in the ultrasonic range suggests that metaconcrete could be used for mitigating explosions or impacts caused by impulsive external forces that activate a wide range of frequencies. Metaconcrete could be employed in the field of Civil Engineering as explosive blast shielding structures, protective slabs against impacts, and tuned damping foundations to mitigate seismic actions in buildings.

3 MATERIALS AND METHODS

The specimens used in this experiment consist of randomly arranged ultra-high-strength fiber-reinforced concrete. These specimens were prepared for investigation under the title "Analysis of the tensile fracture properties of ultra-high-strength fiber-reinforced concrete with different types of steel fibers using X-ray tomography" [12].

This chapter explains the detailed composition of the specimens, along with the execution of the experiment, the equipment utilized, and the processing of the results obtained.

3.1 Specimens: concrete mix and fibers

Four mixes of ultra-high-strength fiber-reinforced concrete (UHSFRC) were prepared. The mortar in all four mixes was the same, with variations only in the type and proportion of fibers used for reinforcement.

Two different types of fibers were used, show in *Figure 3.1*:

- Micro-fibers: straight and short fibers of OL 13/.20, 13 mm in length and 0.20 mm in diameter [12].
- Macro-fibers: long and hooked-end Dramix RC80/30CP, 35 mm in length and 0.55 mm in diameter [12].

(a) *(b)*

Figure 3.1: fibers used as reinforcement in the specimens;
(a) short fibers, (b) long fibers

The concrete matrix mix is detailed in *Table 3.1,* designed to achieve self-compacting mixes with a high density of silica fume, resulting in a dark color. Further information on the fabrication of the specimens and their components can be found in the referenced article. The four types of specimens achieved compression strengths ranging approximately between 130 and 150 MPa, with Young's modulus values ranging from 43 to 50 GPa.

Constituent	**kg/m^3**
Cement (cm)	544
Silica fume (0,1µm)	214
Ground granulated blag slag furnace (ggbs)	312
Water (w)	188
Quartz sand (< 315 µm)	470
Quartzsand (< 800 µm)	470
Superplasticizer (BASF Masterglenium)	42
w/ cm	0.34
w/ binder	0.17

Table 3.1: Constituents of the matrix for the different UHSFRC mixes [12]

The four mixes prepared were labeled based on the type of fibers used, as reported in *Table 3.2*. Mix D0 represents concrete without fibers and serves as the reference specimen. Mixes DS and DL contain 2.5% by volume of short and long fibers, respectively. The specimen labeled DSL is a hybrid mix with a 50% - 50% ratio of short and long fibers. All inclusions were randomly arranged. Regarding the fiber dosage for each type of specimen, it is detailed in *Table 3.2* as well.

Specimen	**Fiber type**	**Fiber dosage (kg/m3)**
D0	No fibers	0
DS	Micro-fibers	196
DL	Macro-fibers	196
DSL	Micro- (50%) and macro-fibers (50%)	98 / 98

Table 3.2: UHSFRC mixes and fiber dosage [12]

Each of these specimens was further divided into four pieces to allow for a statistical evaluation of their behavior. Thus, a total of 16 cubic samples were obtained (*Figure 3.2*).

Figure 3.2: samples of the four types of specimens (D0, DS, DL an DSL)

3.2 Experimental Setup

The experimental campaign involves subjecting four different types of specimens to high-frequency vibrations to observe their damping behavior and determine if resonance occurs in the fibers.

The setup includes:

- Two wooden supports for the concrete specimens (*Figure 3.3 (a)*);
- A Duokon vibration speaker used as an actuator (*Figure 3.3 (b)*);
- Two high frequency, ceramic shear ICP® accel., 10 mV/g, 5 to 60k Hz, 5-44 top conn. (*Figure 3.3 (c)*);
- Two low-noise coaxial cable, 10-ft, micro 5-44 plug to BNC plug (*Figure 3.3 (d)*);
- A SIRIUS-8xACC-8xAO acquisition board (*Figure 3.3 (e)*);
- A laptop running Dewesoft software for data reception and management (*Figure 3.3 (f)*);

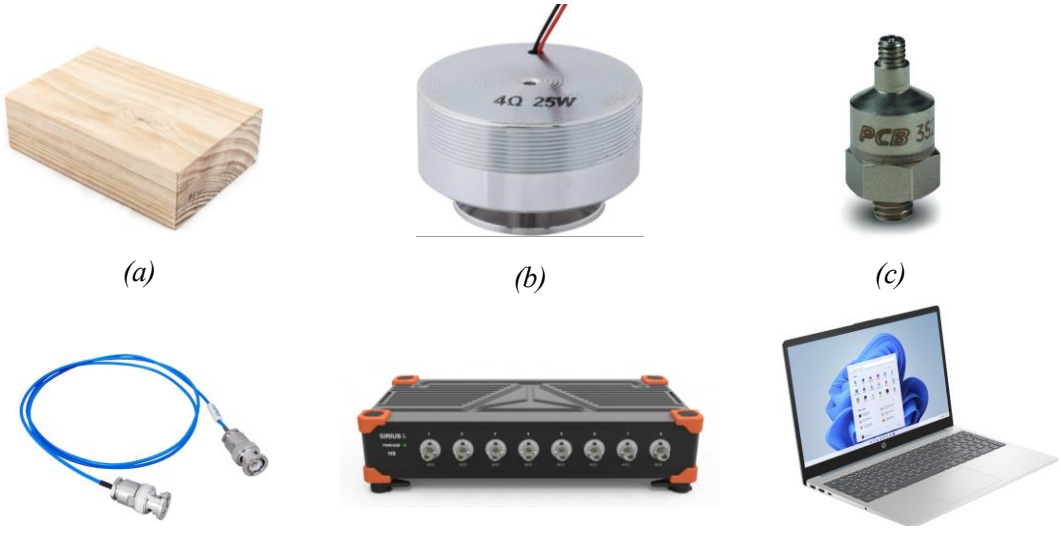

(a) *(b)* *(c)*

(d) *(e)* *(f)*

Figure 3.3: equipment used during the experimental campaign; (a) wooden support, (b) speaker, (c) piezoelectric accelerometer, (d) low-noise cable, (e) acquisition board, (f) laptop with Dewesoft software

In *Figure 3.4*, the hardware used is shown, including accelerometers, cables, bonding putty, wooden supports, and a specimen.

Figure 3.4: picture of equipment used

The wooden supports isolate the specimens from the desk. Two accelerometer readings were collected: one from the bottom surface of the cube opposite to the speaker, labeled as the direct wave (DW), and another from the surface where the speaker was placed, known as the reflected wave (RW). *Figure 3.5* shows the arrangement of both accelerometers. To ensure proper adhesion between the accelerometers and the specimen, a special anchoring wax was used to facilitate wave transmission.

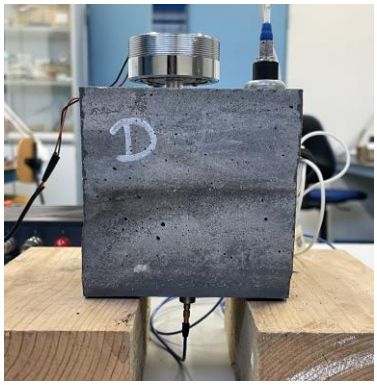

(a)

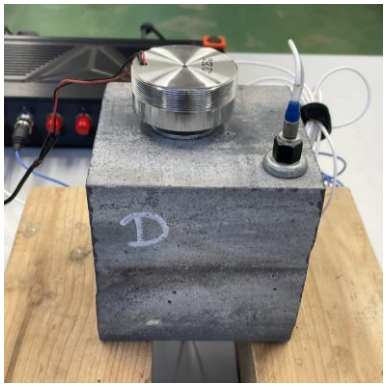

(b)

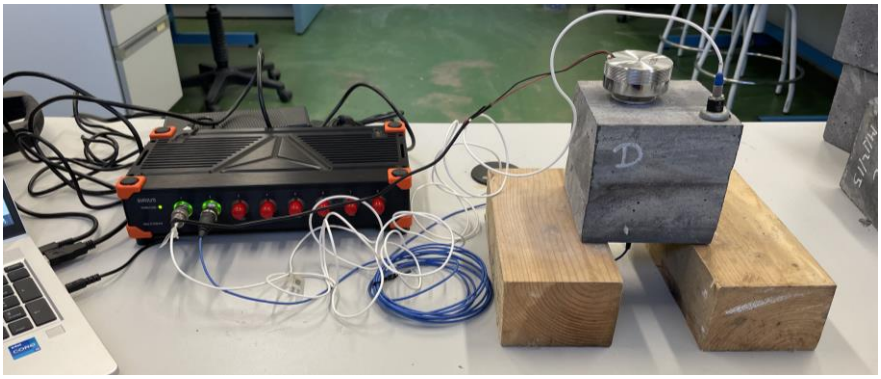

(c)

Figure 3.5: experimental setup arrangements; (a) and (b) placement of upper and lower accelerometer, (c) complete overlook of the analog input

Due to the pioneering nature of this study, we aimed to sweep through a wide range of frequencies. However, we were limited by the speaker's capability, which can only reach up to 25 kHz. To ensure accurate data collection and prevent aliasing, we selected a sampling frequency of 100,000 Hz, which is more than twice the maximum experimental frequency of 25,000 Hz required by the Nyquist sampling theorem. The choice of 100 kHz was determined by the options available in the software used, resulting in a sampling time interval of 1^{-5} seconds.

The frequency sweeps were executed using a Matlab script, where the starting and ending frequencies, along with the time interval, were defined. They were segmented into 5 sweeps, each spanning 10 kHz and lasting 30 seconds to ensure a quasi-static response [13]. Segmentation of the frequency spectrum was necessary due to the large file sizes generated by the high sample rate, which posed challenges for data exportation. The Matlab script mentioned can be found in *section 1.1* of *Appendix.* A schematic representation of the conducted sweeps, including their start and end frequencies, is detailed in *Table 3.3*.

Sweep	**f_e [Hz]**	**f_s [Hz]**	**T [s]**
B1	0	10000	30
B2	5000	15000	30
B3	10000	20000	30
B4	15000	25000	30
B5	20000	30000	30

Table 3.3: frequency sweeps

Each specimen of each type (totaling 16 samples) underwent testing with all frequency sweeps. The computer, connected to the equipment, was positioned on a separate chair to avoid interfering with accelerometer measurements during the start and end of the sweeps. This setup is illustrated from *Figure 3.6* to *Figure 3.9*. Subsequently, the accelerations will be transformed into the frequency domain using the software explained in the following sections.

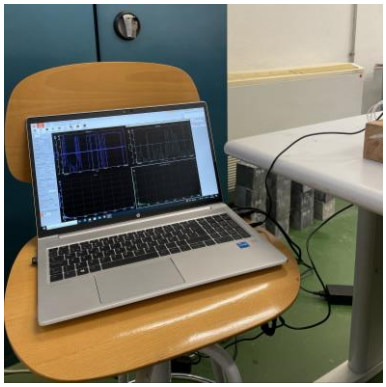

Figure 3.6: laptop placement

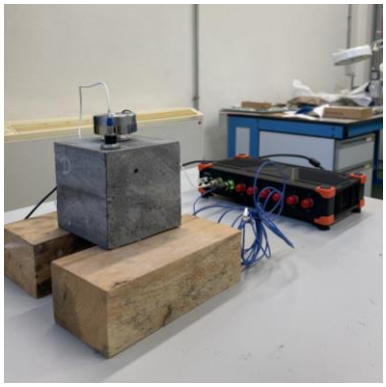

Figure 3.7: experimental setup

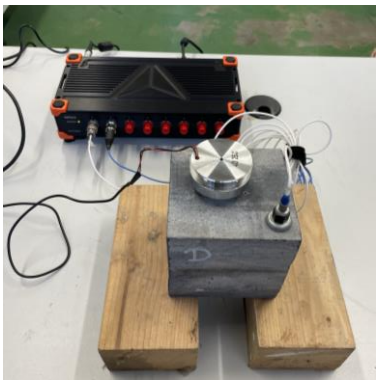

Figure 3.8: channel setup

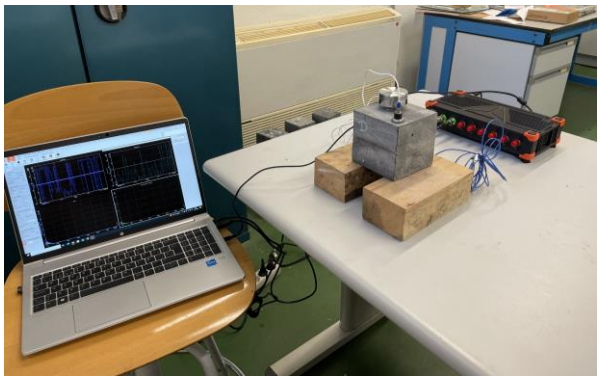

Figure 3.9: complete experimental setup

3.3 Equipment

The data acquisition hardware used for the measurements was the SIRIUS system. It also includes a license for the Dewesoft data acquisition software. For this project, we used the SIRIUS-8xACC-8xAO acquisition board (*Figure 3.11*).

To configurate the software, the first step was to set the channels connected to the accelerometers. Channel 1 (A1) is designated for the reflected wave (RW) and Channel 2 (A2) for the direct wave (DW), as shown in *Figure 3.10*. The white cable connects to channel 1, while the blue cable connects to channel 2.

These channels will measure the accelerations in meters per second squared. The remaining channel configurations are selected based on the recommendations provided in the software manual. *Figure 3.12* shows the configuration for the analog input.

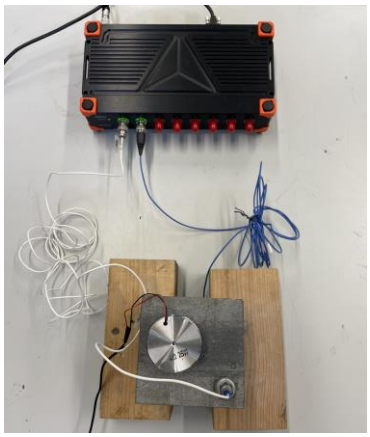

Figure 3.10: channels of analog input setup

Figure 3.11: SIRIUS-8xACC-8xAO acquisition board

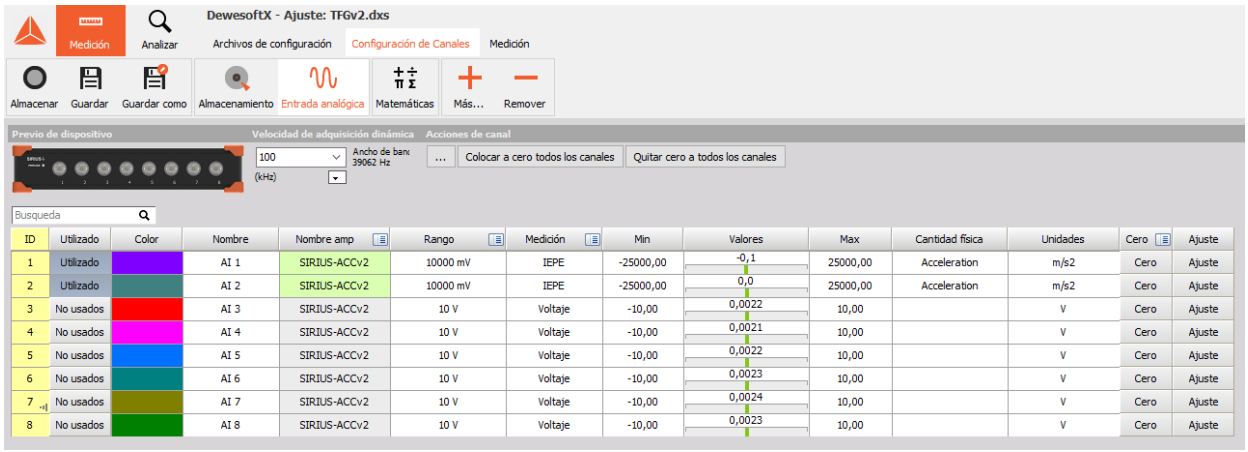

ID	Utilizado	Color	Nombre	Nombre amp	Rango	Medición	Min	Valores	Max	Cantidad física	Unidades	Cero	Ajuste
1	Utilizado		AI 1	SIRIUS-ACCv2	10000 mV	IEPE	-25000,00	-0,1	25000,00	Acceleration	m/s2	Cero	Ajuste
2	Utilizado		AI 2	SIRIUS-ACCv2	10000 mV	IEPE	-25000,00	0,0	25000,00	Acceleration	m/s2	Cero	Ajuste
3	No usados		AI 3	SIRIUS-ACCv2	10 V	Voltaje	-10,00	0,0022	10,00		V	Cero	Ajuste
4	No usados		AI 4	SIRIUS-ACCv2	10 V	Voltaje	-10,00	0,0021	10,00		V	Cero	Ajuste
5	No usados		AI 5	SIRIUS-ACCv2	10 V	Voltaje	-10,00	0,0022	10,00		V	Cero	Ajuste
6	No usados		AI 6	SIRIUS-ACCv2	10 V	Voltaje	-10,00	0,0023	10,00		V	Cero	Ajuste
7	No usados		AI 7	SIRIUS-ACCv2	10 V	Voltaje	-10,00	0,0024	10,00		V	Cero	Ajuste
8	No usados		AI 8	SIRIUS-ACCv2	10 V	Voltaje	-10,00	0,0023	10,00		V	Cero	Ajuste

Figure 3.12: analog input configuration of Channel 1 (RW) and Channel 2 (DW)

While collecting the acceleration data, the software can simultaneously perform the Fast Fourier Transform (FFT) for both sets of acceleration data. To perform this step, it needs to be set in the mathematics section. The configuration followed the software manual, with the options is shown in *Figure 3.13* and *Figure 3.14*.

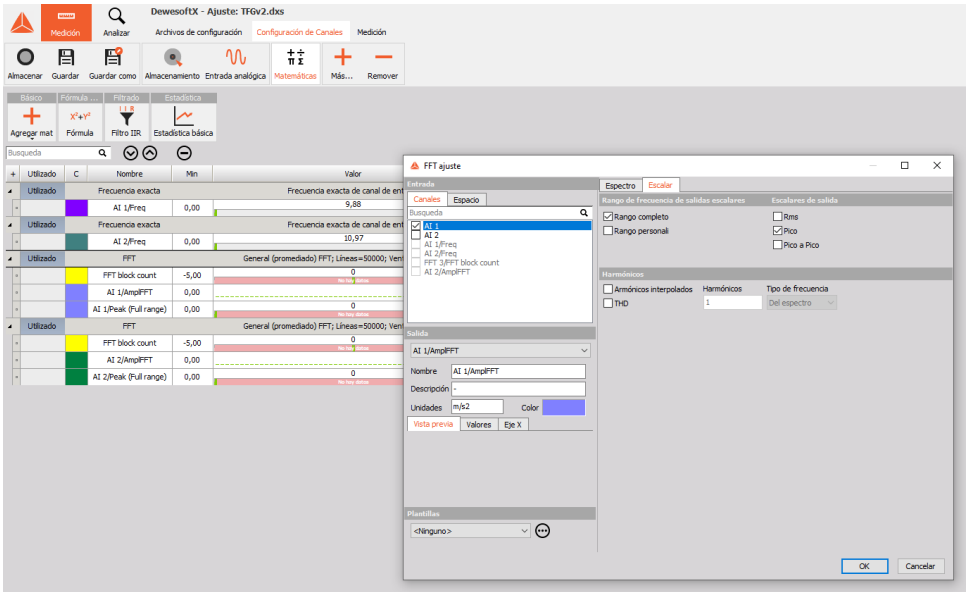

Figure 3.13: FFT configuration in mathematics section

To verify if the frequency measured by the machine matches the frequency programmed for the sweeps, the "exact frequency" option was added to the mathematics tab. Thus, the mathematics tab is set up as follows:

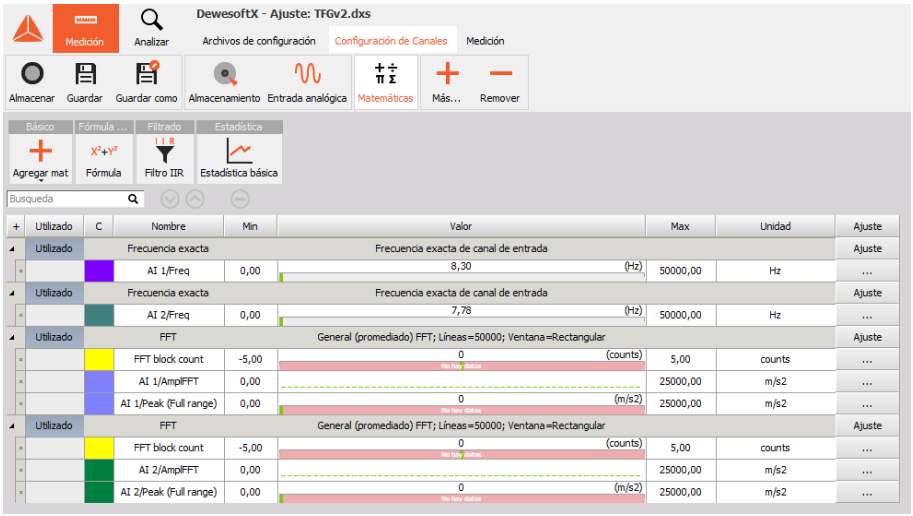

Figure 3.14: mathematics tab configurations

Once the data is obtained, the measurements and calculations can be accessed in the export tab. The chosen format for exporting the data is CSV. The following section explains the data processing in more detail.

3.4 Data processing

For computational reasons, five separate frequency sweeps were performed. However, to provide an overall view of the considered spectrum and facilitate drawing conclusions, the data from these sweeps have been combined into a single graph.

Additionally, the four samples of each type were averaged to produce a single graph for each specimen type (D0, DS, DL and DSL). This approach provides better average data, offering a more accurate description of the behavior of the specimens.

As discussed in *Chapter 2*, the parameter used to evaluate the energy attenuation effectiveness in this study is transmissibility, which measure the energy absorbed by the metaconcrete compared to the homogeneous sample when subjected to dynamic stress that generates an elastic wave. In this context, it is considered a ratio between the acceleration produced in a fiber-reinforced specimen and the reference specimen without fibers.

The core study of this work is based on FFTs, which provide the most relevant information. These FFTs results were exported from the software to Matlab, where two types of scripts were developed:

- Four scripts that averaged the values of the direct and reflected waves in the frequency domain for each specimen type (D0, DS, DL, and DSL) and combined the five sweeps.
- A script that calculated the transmissibility for each specimen type.

3.4.1 FFT averaging

For the four averaging scripts, the first step involved importing all FFT data from the 5 sweeps. Next, the data needed to be sorted for processing due to its exported format. Then, for each wave (RW and DW), the FFTs were averaged across each sweep.

Combining the 5 sweeps into one graphic required considering the overlap between sweeps (*Table 3.3*). This was achieved by averaging the overlapping segments for both waves.

Finally, a moving average was applied to smooth the graph and enhance its interpretability. In this case, the moving average computes the mean for each point using the 25 adjacent points.

The scripts for averaging D0, as an example of the four scripts, can be found in *section 1.2* of *Appendix*. The moving average script is shown in *section 1.2* of *Appendix* as well.

3.4.2 Transmissibility

Transmissibility is represented in logarithmic scale expressed in dB, following the methodology from the thesis of reference [2]. This means calculating the ratio of the average FFT of a metaconcrete specimen (DS, DL and DSL) for each wave (RW and DW) to the average FFT of the specimen without any fibers:

$$T\ (dB) = 20 \cdot \log_{10} \frac{A_i}{A_0} \qquad [3.1]$$

being A_i the average acceleration of the FFT for any of the metaconcrete specimens (DS, DL, and DSL), and A_0 the average acceleration of the FFT for the specimen D0.

The script calculates the three transmissibilities and displays them and can be found in *section 1.3* of *Appendix.*

4 EXPERIMENTAL ANALYSIS

In this chapter, the results obtained after post-processing with the Matlab scripts explained in the previous chapter are reviewed. Each sample provides two measurements: one from the upper surface representing reflected waves and one from the lower surface representing direct waves. The raw data, presented in the form of FFTs, are analyzed and displayed below, as well as the transmissibility.

4.1 Frequency domain

The direct and reflected wave (DW and RW) are represented for each type of specimen (D0, DS, DL and DSL), from *Figure 4.1* to *Figure 4.4* In addition, all types of specimens have been plotted on the same graph for each wave to facilitate better comparison between them (*Figure 4.5* and *Figure 4.6*).

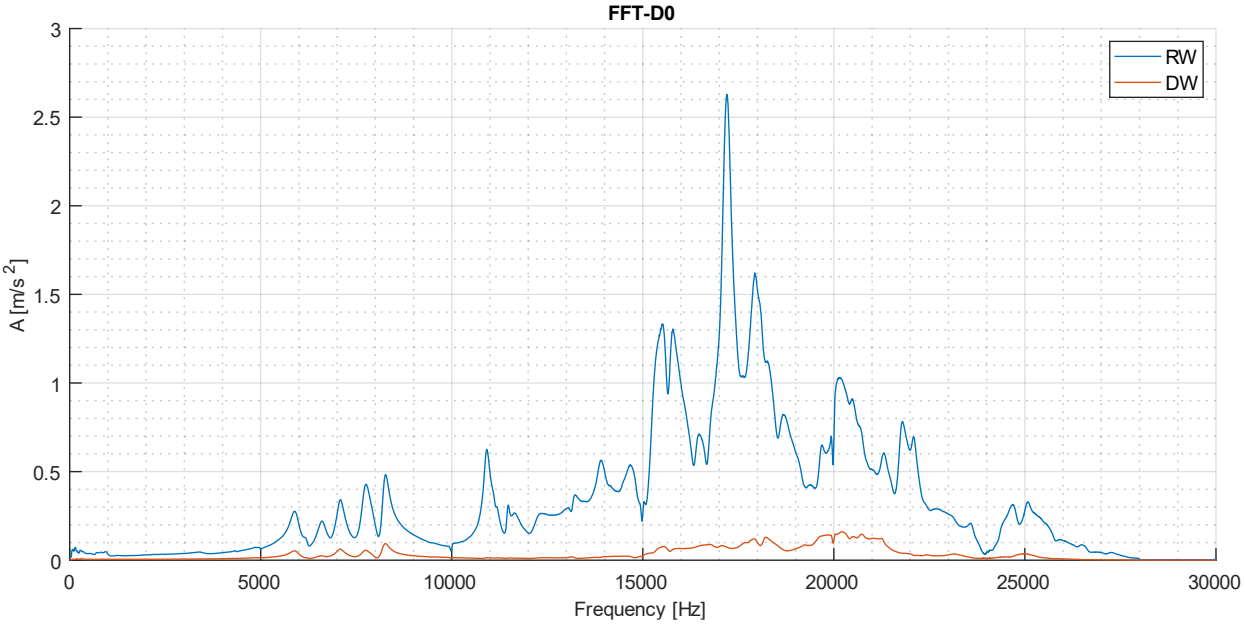

Figure 4.1: frequency domain for the direct and reflected wave of D0 specimen

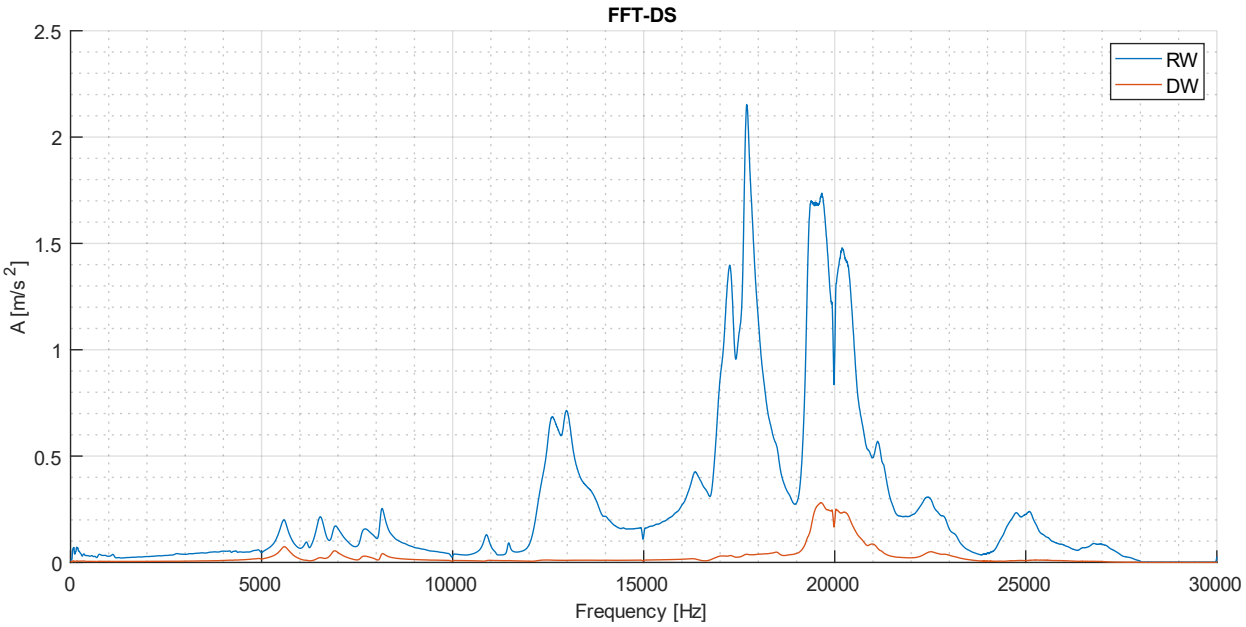

Figure 4.2: frequency domain for the direct and reflected wave of DS specimen

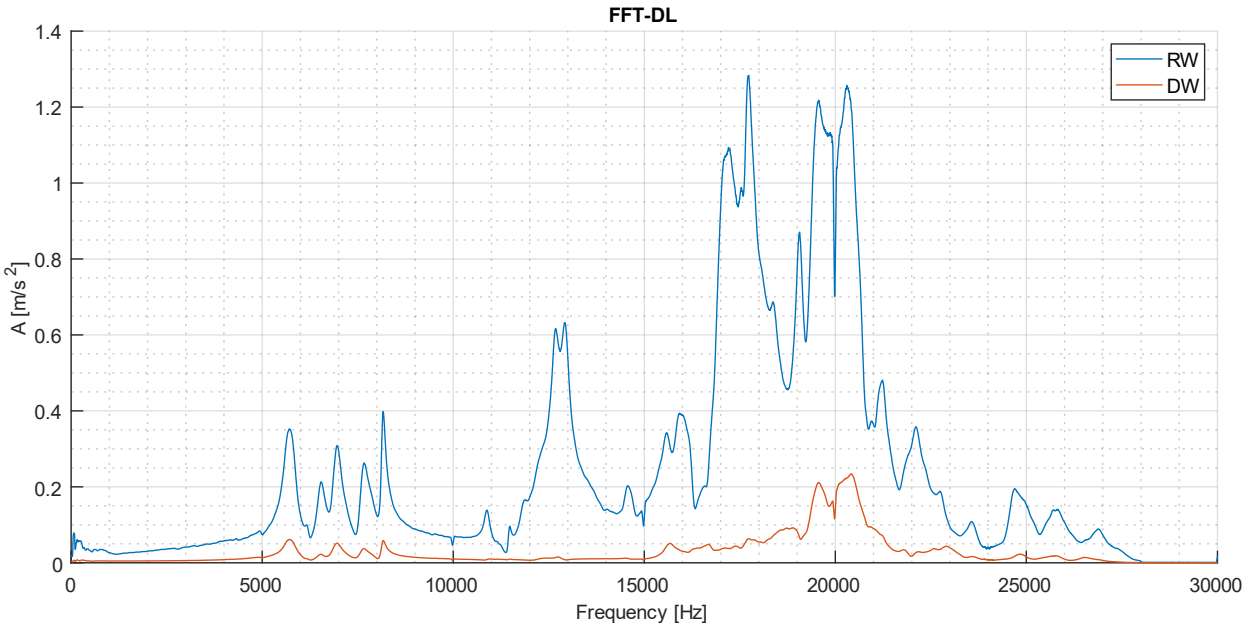

Figure 4.3: frequency domain for the direct and reflected wave of DL specimen

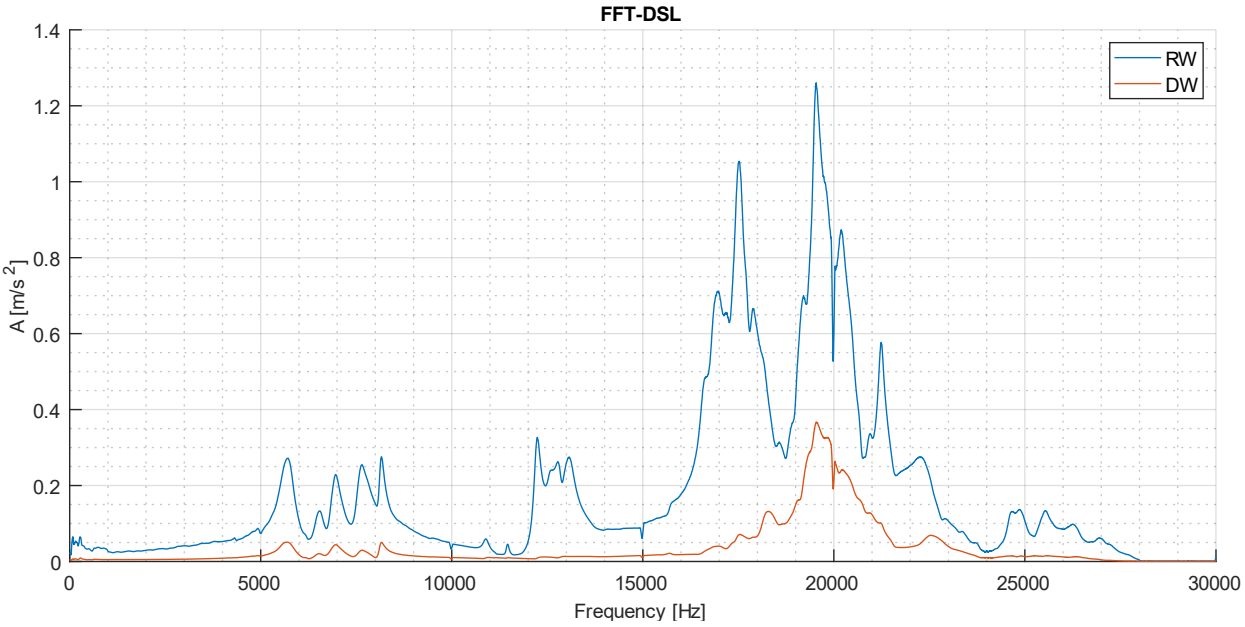

Figure 4.4: frequency domain for the direct and reflected wave of DSL specimen

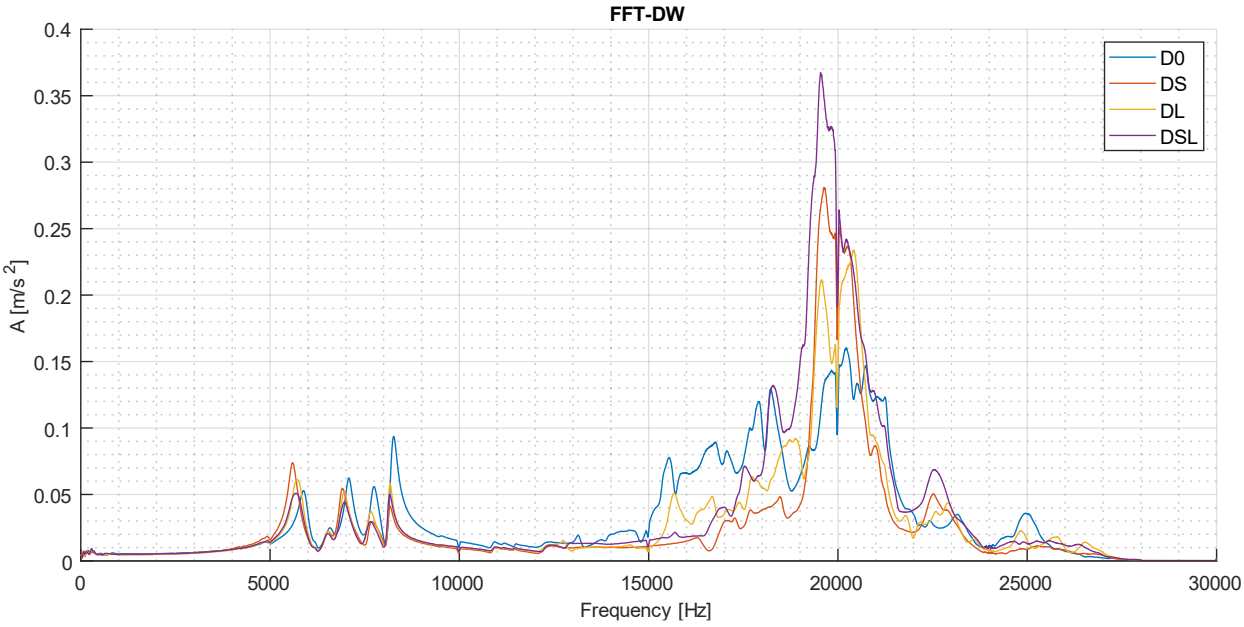

Figure 4.5: frequency domain for the direct wave of all specimens

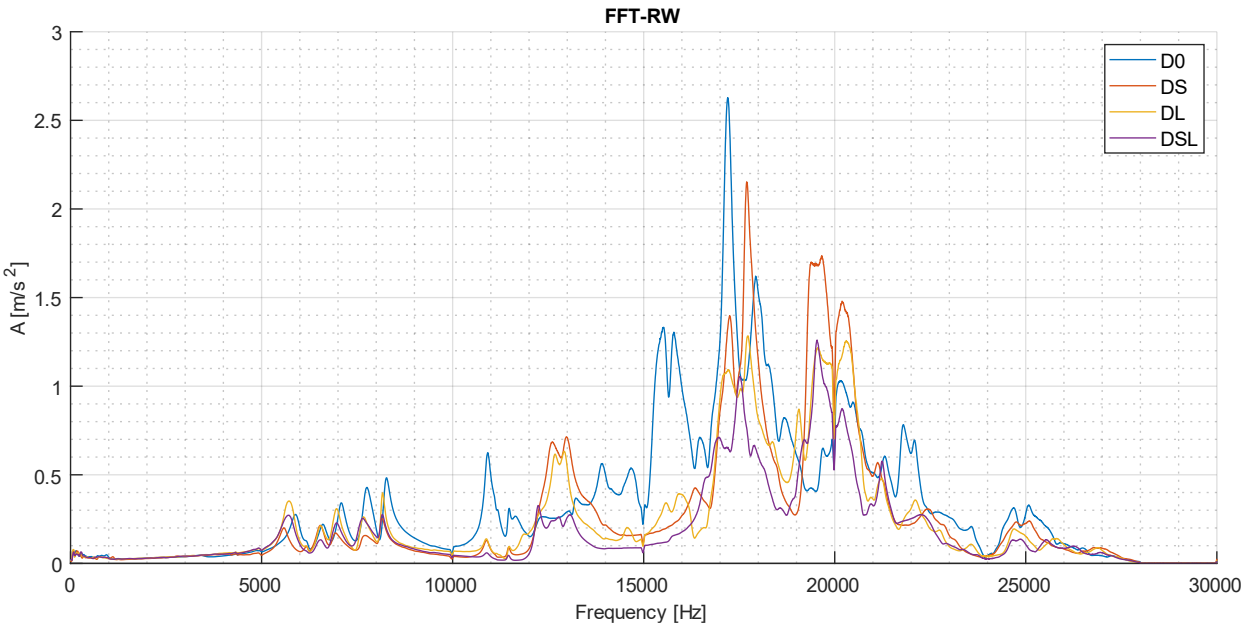

Figure 4.6: frequency domain for the reflected wave of all specimens

It was observed that the measured reflected waves are of greater magnitude than the direct waves. This could be due to the proximity of the accelerometer to the speaker. It could also be influenced by the fact that the samples are quite small compared to other studies conducted. Also, due to the heterogeneous nature of the material, wave propagation can complex, causing the reflected wave to reach the upper accelerometer (RW) before the lower one (DW).

For the analysis of the results, since there is no numerical study backing it up, all frequency ranges and possible effects for all specimens will be discussed.

Up to 5,000 Hz, no response is observed for either the specimen without inclusions or the metaconcrete specimens (*Figure 4.5* and *Figure 4.6*).

Between 5,000 Hz and 10,000 Hz, there is a slight acceleration observed in both the D0 specimen and the metaconcretes, all showing very similar values. In the next chapter, these results will be discussed in more detail and better illustrated.

Between 10,000 Hz and 15,000 Hz, there is a distinction between direct and reflected waves. The direct wave shows minimal response (*Figure 4.5*). However, in the reflected wave around 12,500 Hz, the metaconcrete specimens exhibit excitation (*Figure 4.6*). The DS specimen experiences the highest acceleration (*Figure 4.2*), followed by DL (*Figure 4.3*) and DSL (*Figure 4.4*). Specimen D0 maintains some acceleration throughout this range (*Figure 4.1*). For frequencies around 11,000 Hz and 14,000 Hz, a decrease in accelerations is observed compared to the specimen without fibers.

Between 15,000 Hz and 20,000 Hz, there is a significant increase in accelerations for both direct and reflected waves. The direct wave accelerations increase steadily, reaching their peak at 20,000 Hz (*Figure 4.5*). DSL generally experiences the highest accelerations in this range for the direct wave. Specimen D0 also increases its accelerations in this range, peaking at 20,000 Hz but to a smaller value. In the reflected wave, D0 shows peaks near 15,000 Hz and around 17,500 Hz, reaching its global maximum at this point (*Figure 4.6*). Metaconcrete specimens show an increase up to 17,500 Hz, with DS experiencing the highest accelerations. There is also an increase at 20,000 Hz, similar in magnitude to that at 17,500 Hz. For the reflected wave near 15,000 Hz, a significant decrease in accelerations is observed in the metaconcrete specimens compared to specimen D0. Direct wave also shows a decrease in accelerations for metaconcretes between 15,000 Hz and 17,500 Hz, although not as drastic as in the reflected wave.

Between 20,000 Hz and 22,500 Hz, there is a decrease in accelerations for both waves and all specimens (*Figure 4.5* and *Figure 4.6*). Around 22,500 Hz, there is a slight but minor increase observed. Comparing the metaconcretes specimens with the D0 specimen, there is not a significant decrease in accelerations observed.

4.2 Transmissibility

The quantitative observations are possible with the parameter of transmissibility. This parameter captures the mitigation on the accelerations compares to another of reference. In this case, the homogeneous specimen (D0) with no inclusions was used.

The significance of the parameter requires an appropriate discussion, which will be presented following the results. Transmissibility is calculated for each type of specimen and for direct and reflected wave; therefore, we have three graphics (*Figure 4.7*, *Figure 4.8* and *Figure 4.9*). Subsequently, all types of fibers are represented together to facilitate easier comparison of the results between them. (*Figure 4.10* and *Figure 4.11*).

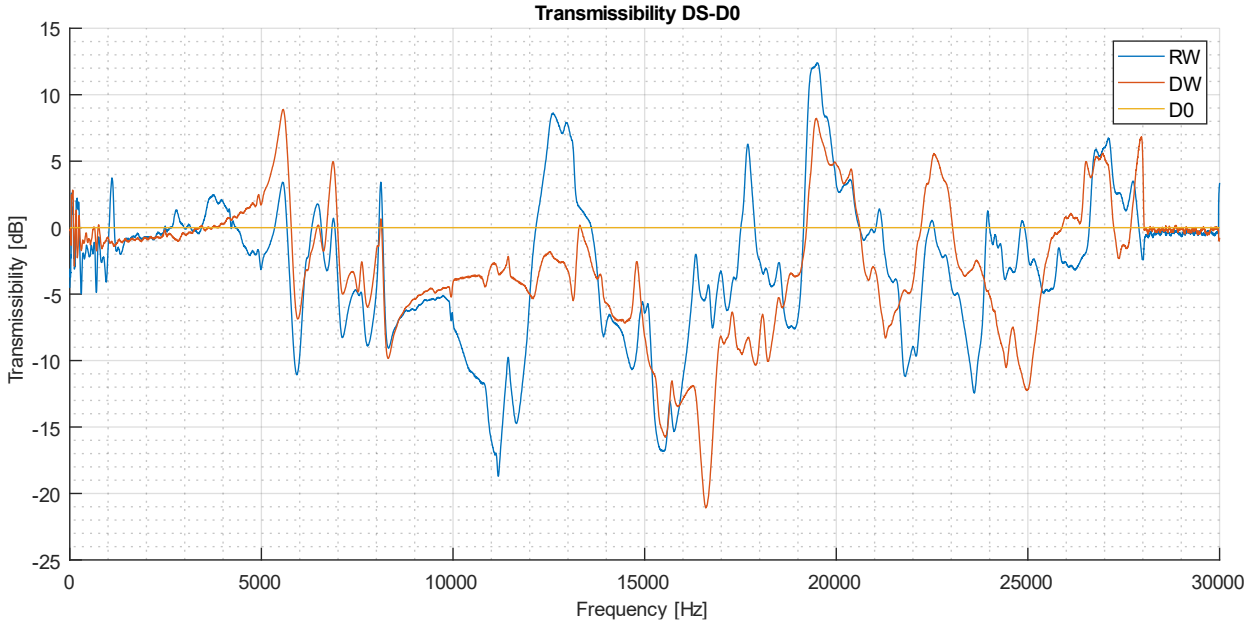

Figure 4.7: transmissibility of the direct and reflected wave of DS specimen

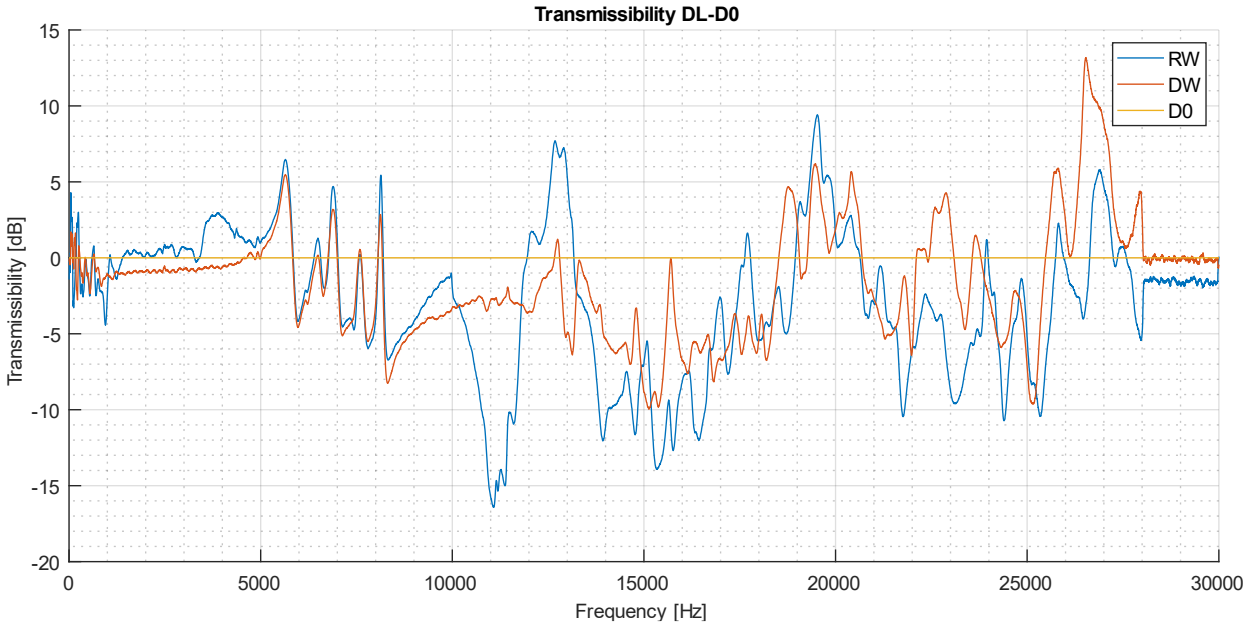

Figure 4.8: transmissibility of the direct and reflected wave of DL specimen

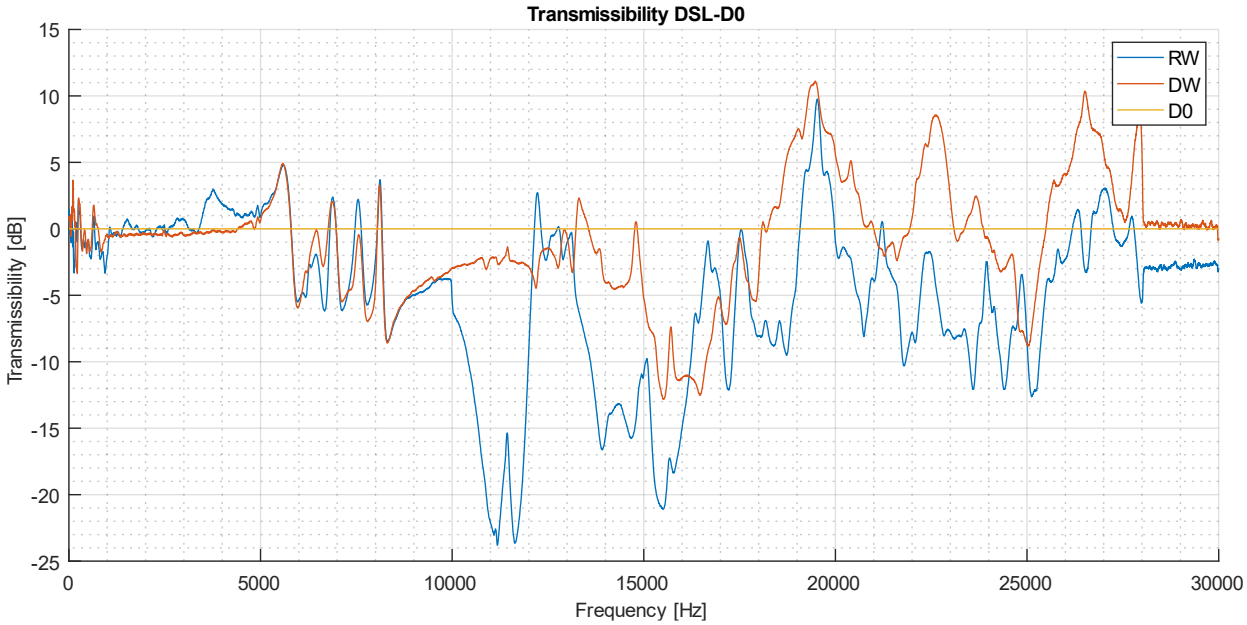

Figure 4.9: transmissibility of the direct and reflected wave of DSL specimen

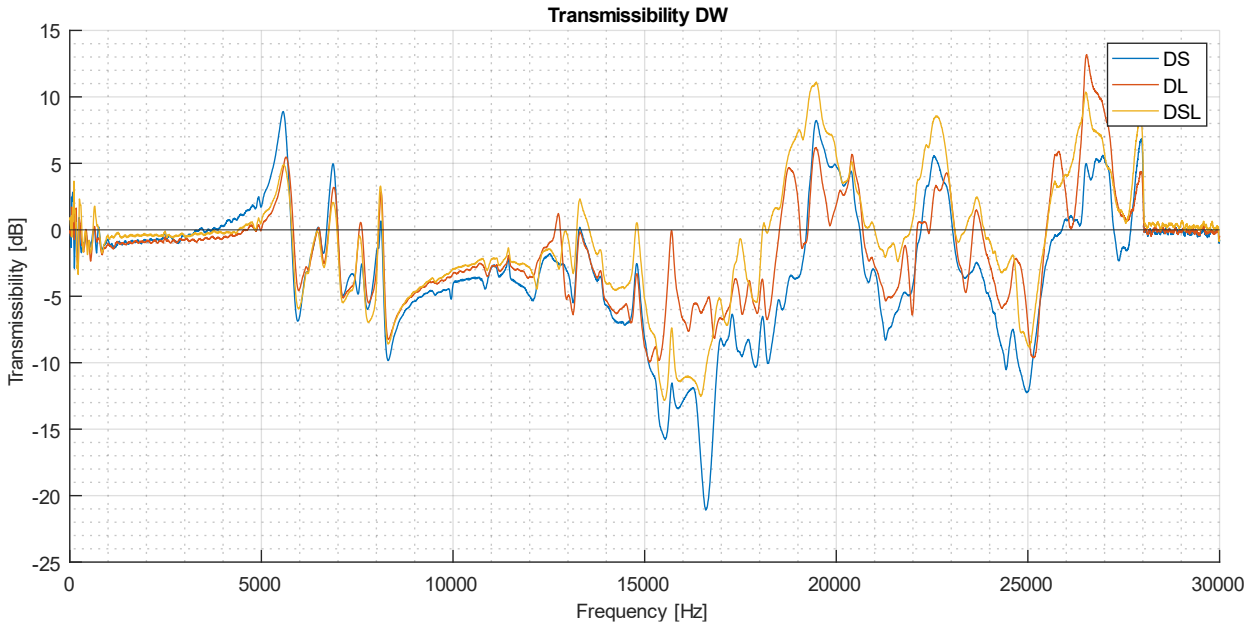

Figure 4.10: transmissibility of the direct wave of all metaconcrete specimen

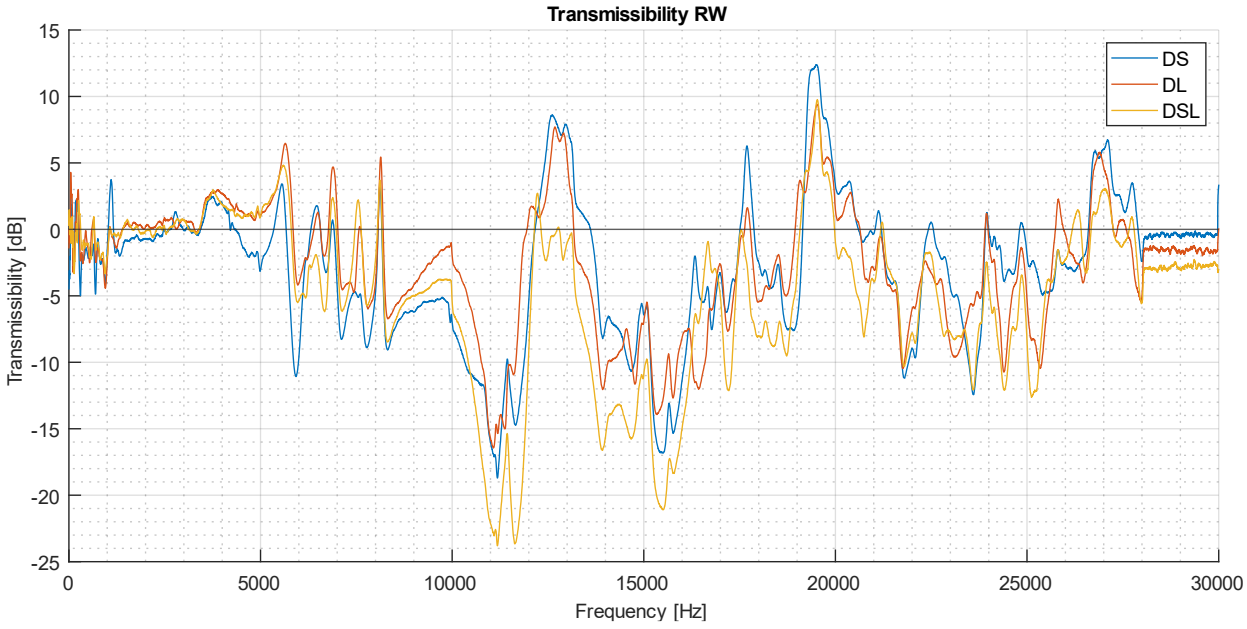

Figure 4.11: transmissibility of the reflected wave of all metaconcrete specimen

As indicated in the thesis of reference [2], transmissibility represents a significant index of signal attenuation only if the frequency range considered is not affected by global resonance phenomena of the specimens. However, since there are no clear data on global resonance ranges, the entire frequency range is being analyzed.

For the range up to 5,000 Hz, no remarkable effects were observed, attributing the initial turbulences to possible effects of the experimental setup (*Figure 4.10 and Figure 4.11*).

In the range between 5,000 Hz and 10,000 Hz, inconsistent decreases in transmissibility were observed, with specimen DS showing the highest value. (*Figure 4.7*).

In the range between 10,000 Hz and 15,000 Hz, different responses were observed for the reflected and direct waves. For the direct wave, a slight decrease in transmissibility was noticed. (*Figure 4.10*). However, for the reflected wave, the most significant decrease occurred around 11,000 Hz. This abrupt decrease is attributed to the hybrid specimen with short and long fibers. This effect was also visible in *Figure 4.6*.

For values between approximately 14,000 Hz and 17,000 Hz, significant decreases in transmissibility were also observed. For the direct wave, these occur closer to 17,000 Hz, with DS showing the highest value followed by DSL. For the reflected wave, the decrease is centered more around 15,000 Hz, with DSL showing the largest decrease followed by DS.

From 20,000 Hz onwards, decreases in transmissibility are observed, but they are more inconsistent and of lesser magnitude. However, around 25,000 Hz, the direct wave experiences a noticeable decrease, with DS showing the highest value. Similar decreases in transmissibility are also observed for the reflected wave around this frequency range.

5 DISCUSSION OF RESULTS

In this chapter, the analyzed results will be discussed. Additionally, close-ups of the graphs will be provided within the frequency ranges of interest to facilitate better interpretation. In the frequency domain, two ranges of interest were identified: from 5,000 Hz to 10,000 Hz and from 15,000 Hz to 20,000 Hz. Below is presented the first range for direct and reflected waves of all specimens.

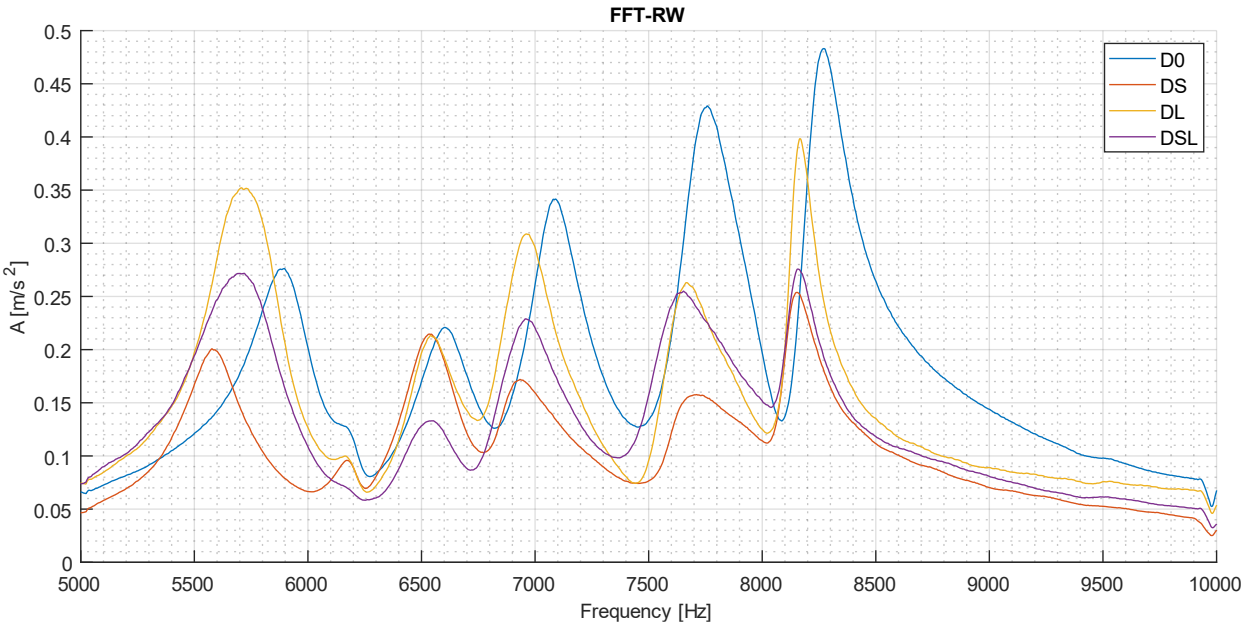

Figure 5.1: frequency domain for the reflected wave of all specimens between 5,000 Hz and 10,000 Hz

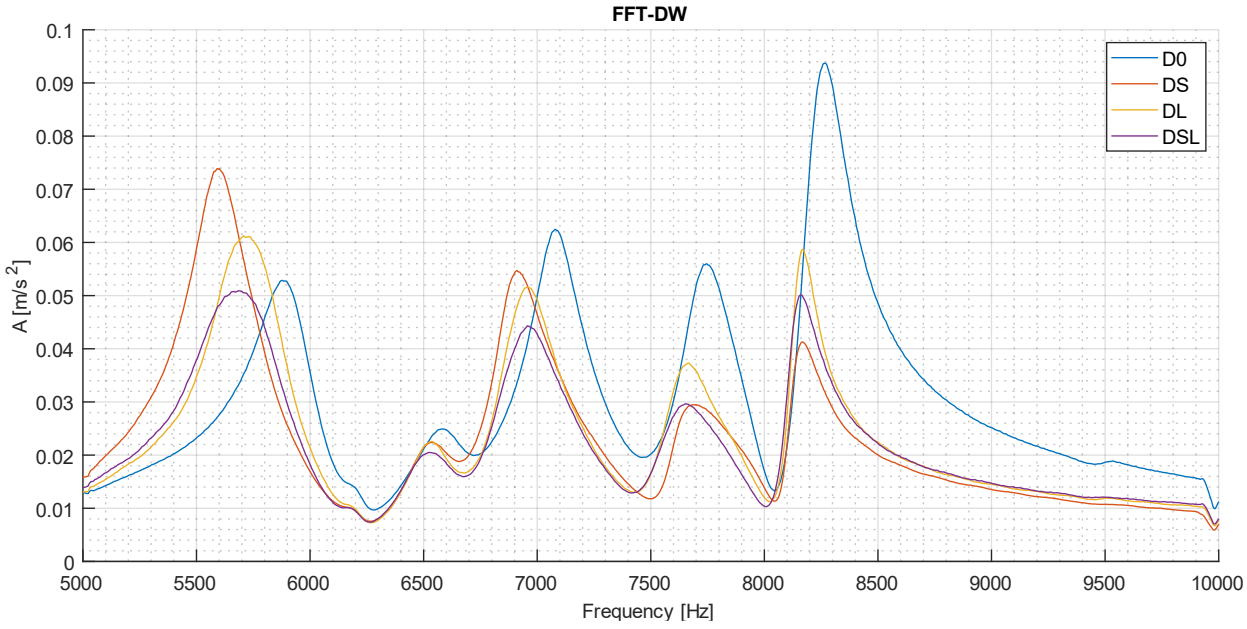

Figure 5.2: frequency domain for the direct wave of all specimens between 5,000 Hz and 10,000 Hz

For both waves, a similar trend is observed. As the frequencies increase, the reduction of accelerations associated with the metaconcretes also increases. For accelerations near 5,500 Hz and 6,000 Hz, no attenuation is observed in the metaconcretes, and there is even an increase in accelerations (*Figure 5.1* and *Figure 5.2*). For frequencies around 7,750 Hz and 8,250 Hz, a slight decrease in accelerations is observed in the metaconcrete specimens. In this range, greater attenuation is achieved at 8,250 Hz in the specimens with short fiber and hybrid (DS and DSL).

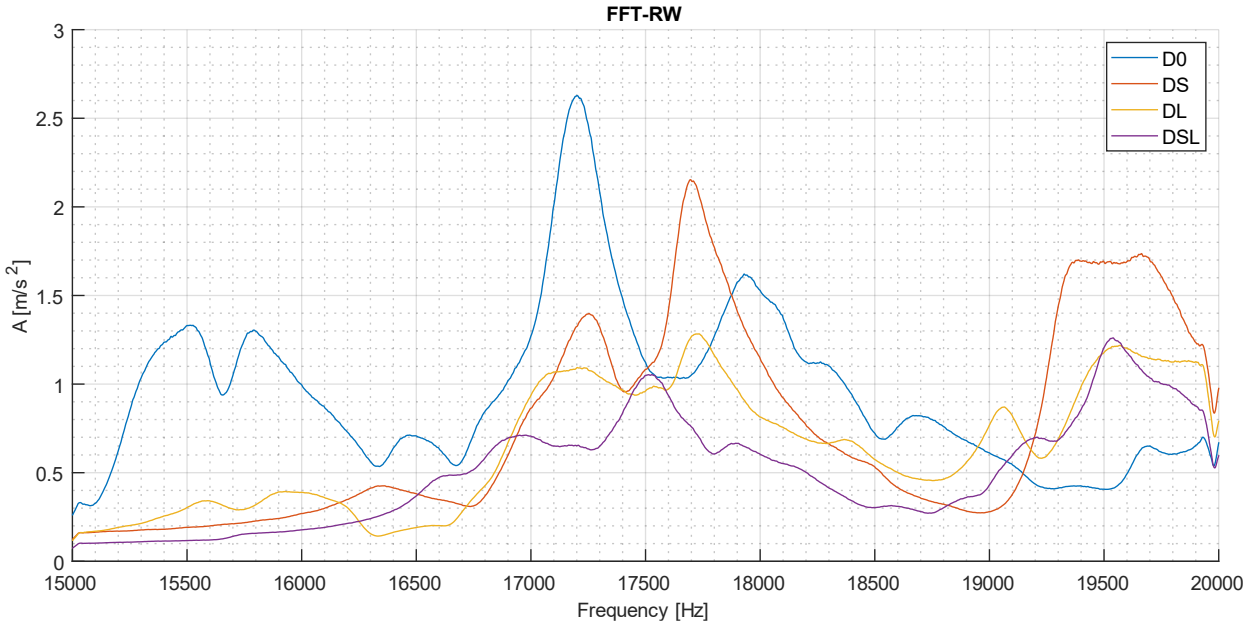

Figure 5.3: frequency domain for the reflected wave of all specimens between 15,000 Hz and 20,000 Hz

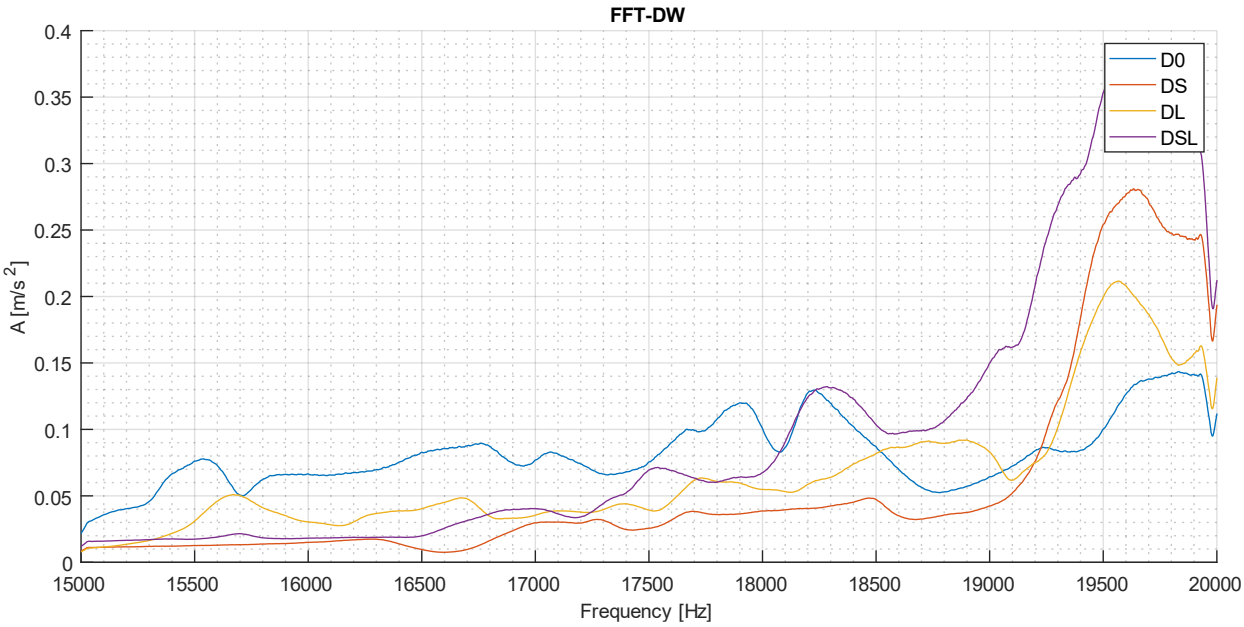

Figure 5.4: frequency domain for the direct wave of all specimens between 15,000 Hz and 20,000 Hz

For the range between 15,000 Hz and 20,000 Hz, different responses are observed for the direct and reflected waves. Regarding the reflected wave, a trend is observed up to 17,500 Hz where the metaconcretes register lower accelerations than conventional concrete (D0). This trend continues up to approximately 19,000 Hz, despite a change around 17,750 Hz where an increase in accelerations is recorded in the short and long fiber metaconcrete (DS and DL) compared to conventional concrete. Between 19,000 Hz and 20,000 Hz, significantly higher accelerations are observed in the metaconcretes (DS, DL, and DSL) compared to the D0 specimen.

Regarding the direct wave, slight decreases in accelerations are observed for all metaconcretes up to 18,250 Hz. Beyond this frequency, higher accelerations start to be recorded in the DSL specimen. At 18,500 Hz, the DL specimen also begins to show increased accelerations, followed by the DS specimen at 19,250 Hz. This trend, where the metaconcretes register higher accelerations than the reference concrete, continues up to approximately 21,000 Hz (*Figure 4.5* and *Figure 4.6*).

As previously explained, the project aims to assess whether metaconcrete specimens exhibit an attenuating effect compared to traditional concrete specimens without reinforcing fibers. Significant reductions in transmissibility have been observed at various frequencies.

At lower frequencies (between 5,000 Hz and 10,000 Hz), it is observed that the specimen with short fibers attenuates both the reflected and direct waves the most. As shown in *Figure 5.5*, the reflected wave reaches an attenuation of -10 dB around 6,000 Hz. A similar value is also reached for both waves between 8,000 Hz and 8,500 Hz. Given that a response is observed in all specimens, including the one without fibers, it cannot be confirmed that these frequencies are not a global mode of vibration. However, it is observed that metaconcrete slightly attenuates the accelerations at these frequencies.

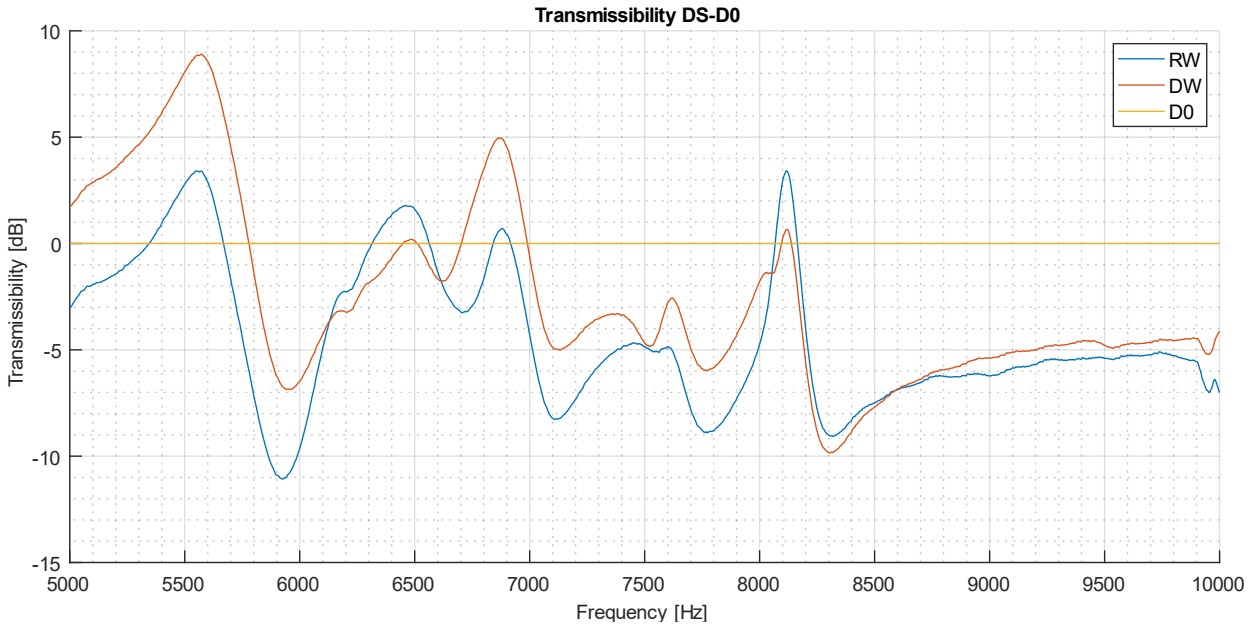

Figure 5.5: transmissibility of the reflected and direct wave in DS specimen between 5,000 Hz and 10,000 Hz

For the reflected wave, a significant attenuation is clearly observed around 11,000 Hz (*Figure 5.6*). In this case, the greatest attenuation is provided by the specimen with both short and long fibers (DSL), followed by the specimen with only short fibers (DS). The attenuations achieved reach nearly -25 dB, making them the highest attenuations recorded in the entire experiment. The attenuations caused by the specimens with only one type of fiber range between -10 dB and -15 dB.

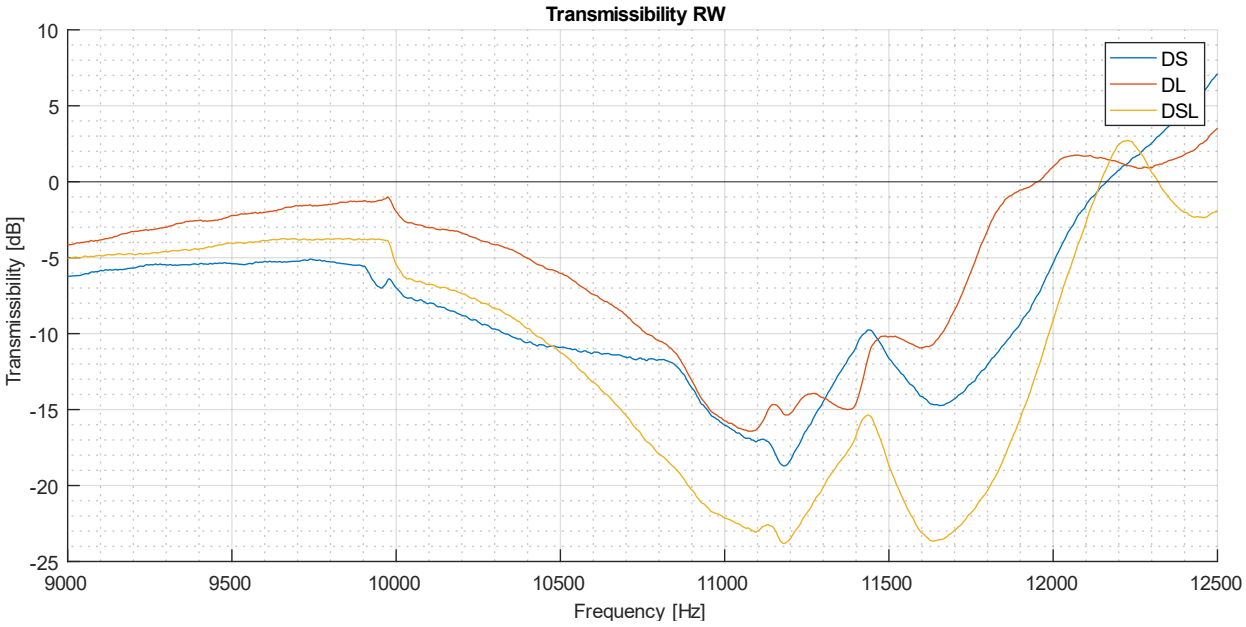

Figure 5.6: transmissibility of the reflected wave in all specimens at around 11,000 Hz

Around 15,000 Hz, attenuations are observed in both waves. For the reflected wave, the largest attenuations are observed at approximately 15,500 Hz (*Figure 5.7*). As observed at previous frequencies, the greatest attenuation is provided by DSL, reaching just over -20 dB. DS and DL show similar values of around -15 dB. Regarding the direct wave, attenuations reach a maximum at 16,500 Hz, with -20 dB (*Figure 5.8*). In this case, the specimen with short fibers shows the highest attenuation. At that frequency, DSL exhibits a response similar to DS, but with an attenuation reaching -12 dB.

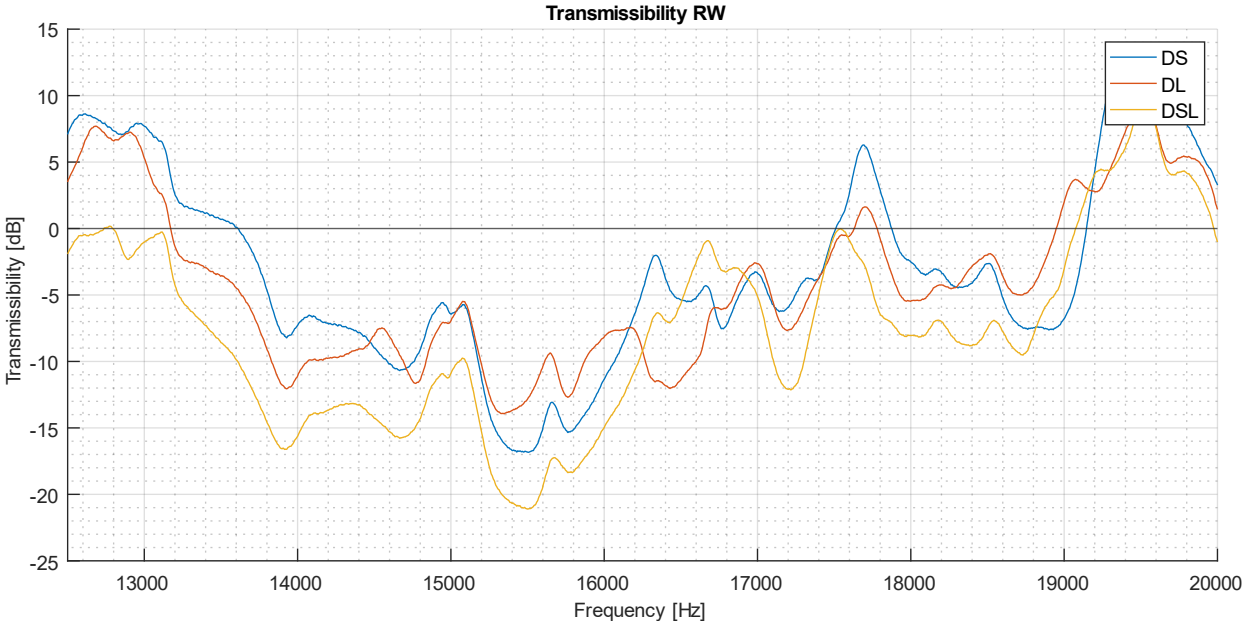

Figure 5.7: transmissibility of the reflected wave in all specimens between 13,000 Hz and 20,000 Hz

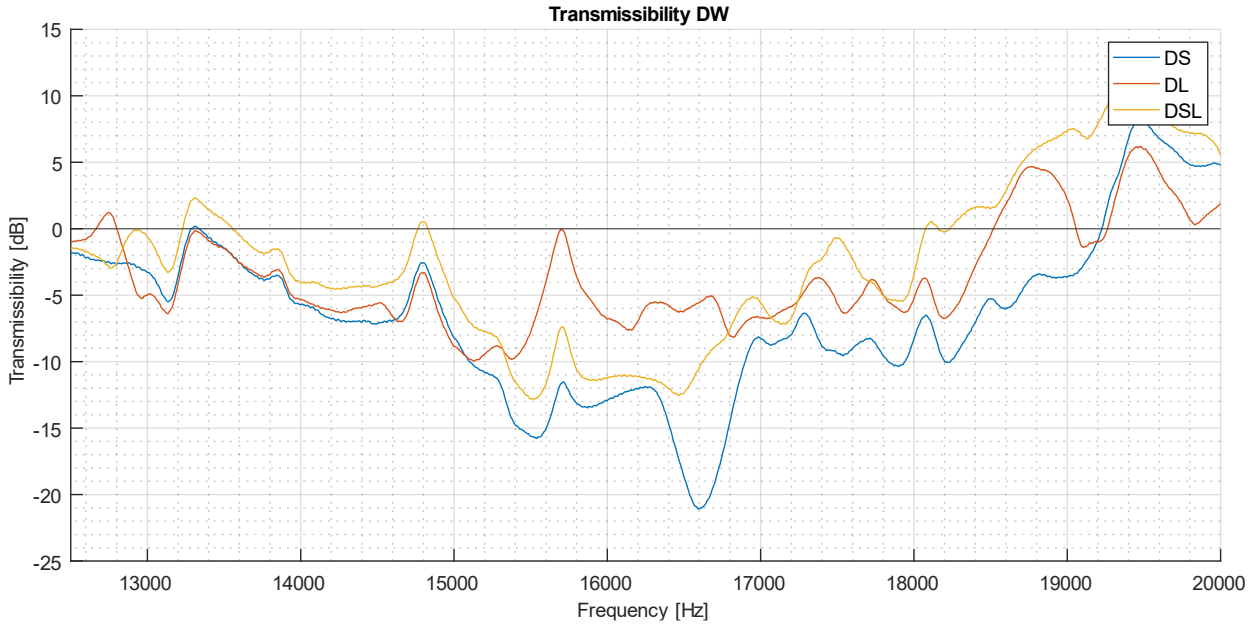

Figure 5.8: transmissibility of the direct wave in all specimens between 13,000 Hz and 20,000 Hz

From 20,000 Hz onwards, there is an attenuating trend observed in both specimens. However, it is in the reflected wave where a clearer attenuation is observed in that range (*Figure 5.9*). This range shows no clear improvement observed among specimens. At frequencies 22,000 Hz and 23,500 Hz, greater attenuation is observed in the specimen with short fibers, achieving -11 dB and -12 dB respectively. Between 20,500 Hz and 21,000 Hz, and near 24,500 Hz, a better performance is observed in the mixed specimen, achieving attenuations of -8 dB and -12 dB respectively.

Figure 5.9: transmissibility of the reflected wave in all specimens between 20,000 Hz and 25,000 Hz

6 CONCLUSIONS AND FUTURE INVESTIGATIONS

In nearly all the mentioned frequencies, greater attenuation was observed in the specimen with short fibers (DS) or in the mixed specimen (DSL). For the study conducted on tensile fracture properties in these specimens [12], the best results were obtained for these two specimens. For improved fracture behavior, it was observed that the mixed specimen performed the best, while from a mechanical point of view, the specimen with short fibers exhibited superior behavior.

In the case of the dynamic damping properties of metaconcrete, a similar situation is observed. Both specimens exhibit the best behaviors, each at specific frequencies. No significant attenuation has been led by the specimen with only long fibers.

When considering the practical application of these metaconcretes in construction, one must consider the costs of constituents and manufacturing for each type. The price of short fibers is higher than that of long fibers [12]. This makes the use of mixed metaconcretes, which show good results and are also more economical, a potentially more optimal solution.

Based on the discussion of results, the following conclusions can be drawn depending on the frequency range:

- For frequency ranges between 5,000 Hz and 10,000 Hz metaconcrete specimens show an overall reduction in the recorded accelerations compared to traditional concrete without fibers.
- For frequencies above approximately 19,000 Hz and up to approximately 21,000 Hz, an increase in accelerations is observed in the metaconcrete specimens.
- The mixed specimen (DSL) and the specimen with short fibers (DS) exhibit greater attenuation across all the attenuated frequencies.
- The specimen with long fibers (DL) attenuates transmitted waves, but to a lesser extent than the other specimens.
- Considering practical applications in construction, the higher cost of short fibers suggests that mixed metaconcretes may provide a more cost-effective solution while maintaining performance standards.

These conclusions indicate that the choice of metaconcrete type should be based on specific project requirements and cost considerations in construction applications.

Despite conducting this project and experimental campaign as accurately as possible, the results have been limited by certain factors. For further research continuation, the following factors could be considered to obtain more complete and conclusive results:

- Use advanced numerical modeling techniques to predict and optimize metaconcrete performance based on inclusions geometry and material properties.
- Conduct similar experimental campaigns with other types of fibers of different geometries and materials.
- Expand the range of excitation frequencies to achieve more comprehensive results.
- Conduct large-scale tests to validate metaconcrete performance in real-world applications requiring vibration attenuation.
- Explore cost-effective strategies for incorporating metaconcrete into construction practices while maintaining performance standards.

REFERENCES

[1] S. J. Mitchell, A. Pandolfi, and M. Ortiz, “Investigation of elastic wave transmission in a metaconcrete slab,” *Mechanics of Materials*, vol. 91, no. P1, pp. 295–303, Dec. 2015, doi: 10.1016/j.mechmat.2015.08.004.

[2] D. Briccola and A. Pandolfi, “Metaconcrete: indagine sperimentale su campioni con inclusioni disomogenee”.

[3] Z. Liu *et al.*, “Locally resonant sonic materials,” *Science (1979)*, vol. 289, no. 5485, pp. 1734–1736, Sep. 2000, doi: 10.1126/science.289.5485.1734.

[4] S. J. Mitchell, A. Pandolfi, and M. Ortiz, “Metaconcrete: designed aggregates to enhance dynamic performance,” *J Mech Phys Solids*, vol. 65, no. 1, pp. 69–81, Apr. 2014, doi: 10.1016/J.JMPS.2014.01.003.

[5] M. S. Kushwaha, ’ P Halevi, ’ L Dobrzynski, and B. Djafari-Rouhani, “Acoustic Band Structure of Periodic Elastic Composites,” 1993.

[6] A. D. Klironomos and E. N. Economou, “ELASTIC WAVE BAND GAPS AND SINGLE SCATTERING,” 1998.

[7] W. H. Bragg, W. L. Bragg Apr, B. W. H Bragg, and C. Professor of Physics, “The Reflection o f X-rays by Crystals.” [Online]. Available: https://royalsocietypublishing.org/

[8] J. V Sánchez-Pérez *et al.*, “Sound Attenuation by a Two-Dimensional Array of Rigid Cylinders,” 1998.

[9] Z. Liu, C. T. Chan, P. Sheng, A. L. Goertzen, and J. H. Page, “Elastic wave scattering by periodic structures of spherical objects: Theory and experiment.”

[10] G. W. Milton and J. R. Willis, “On modifications of Newton’s second law and linear continuum elastodynamics,” *Proceedings of the Royal Society A: Mathematical, Physical and Engineering Sciences*, vol. 463, no. 2079, pp. 855–880, Mar. 2007, doi: 10.1098/rspa.2006.1795.

[11] J. Mei, Z. Liu, W. Wen, and P. Sheng, “Effective dynamic mass density of composites,” *Phys Rev B Condens Matter Mater Phys*, vol. 76, no. 13, Oct. 2007, doi: 10.1103/PhysRevB.76.134205.

[12] J. D. Ríos, C. Leiva, M. P. Ariza, S. Seitl, and H. Cifuentes, “Analysis of the tensile fracture properties of ultra-high-strength fiber-reinforced concrete with different types of steel fibers by X-ray tomography,” *Mater Des*, vol. 165, Mar. 2019, doi: 10.1016/j.matdes.2019.107582.

[13] G. Gloth and M. Sinapius, “Analysis of swept-sine runs during modal identification,” *Mech Syst Signal Process*, vol. 18, no. 6, pp. 1421–1441, Nov. 2004, doi: 10.1016/S0888-3270(03)00087-6.

APPENDIX

1.1 Frequency sweeps

```
% Definir las variables
duration = 30;    % Duración en segundos del archivo de audio
Fs = 100000;      % Frecuencia de muestreo en Hz
f_start = 0;      % Frecuencia inicial en Hz
f_end = 10000;    % Frecuencia final en Hz

% Crear vector de tiempo
t = 0:1/Fs:duration;

% Crear vector de frecuencias
frequencies = linspace(f_start, f_end, length(t));

% Crear señal de audio
signal = sin(2*pi*frequencies.*t);

% Normalizar la señal
signal = signal / max(abs(signal));

% Escribir la señal a un archivo de audio
audiowrite('barrido_frecuencias_0k10k.wav', signal, Fs);
```

1.2 FFT averaging

1.2.1 D0

```
% LECTURA DE DATOS

% Barrido 1
import_fft_B1_P1=uiimport('C:\Users\Public\Documents\Dewesoft\Ex
ports\D0\FFTs\D0_P1_B1_FFT.csv');
import_fft_B1_P2=uiimport('C:\Users\Public\Documents\Dewesoft\Ex
ports\D0\FFTs\D0_P2_B1_FFT.csv');
import_fft_B1_P3=uiimport('C:\Users\Public\Documents\Dewesoft\Ex
ports\D0\FFTs\D0_P3_B1_FFT.csv');
import_fft_B1_P4=uiimport('C:\Users\Public\Documents\Dewesoft\Ex
ports\D0\FFTs\D0_P4_B1_FFT.csv');

% Barrido 2
import_fft_B2_P1=uiimport('C:\Users\Public\Documents\Dewesoft\Ex
ports\D0\FFTs\D0_P1_B2_FFT.csv');
import_fft_B2_P2=uiimport('C:\Users\Public\Documents\Dewesoft\Ex
ports\D0\FFTs\D0_P2_B2_FFT.csv');
import_fft_B2_P3=uiimport('C:\Users\Public\Documents\Dewesoft\Ex
ports\D0\FFTs\D0_P3_B2_FFT.csv');
import_fft_B2_P4=uiimport('C:\Users\Public\Documents\Dewesoft\Ex
ports\D0\FFTs\D0_P4_B2_FFT.csv');

% Barrido 3
import_fft_B3_P1=uiimport('C:\Users\Public\Documents\Dewesoft\Ex
ports\D0\FFTs\D0_P1_B3_FFT.csv');
import_fft_B3_P2=uiimport('C:\Users\Public\Documents\Dewesoft\Ex
ports\D0\FFTs\D0_P2_B3_FFT.csv');
import_fft_B3_P3=uiimport('C:\Users\Public\Documents\Dewesoft\Ex
ports\D0\FFTs\D0_P3_B3_FFT.csv');
import_fft_B3_P4=uiimport('C:\Users\Public\Documents\Dewesoft\Ex
ports\D0\FFTs\D0_P4_B3_FFT.csv');

% Barrido 4
import_fft_B4_P1=uiimport('C:\Users\Public\Documents\Dewesoft\Ex
ports\D0\FFTs\D0_P1_B4_FFT.csv');
import_fft_B4_P2=uiimport('C:\Users\Public\Documents\Dewesoft\Ex
ports\D0\FFTs\D0_P2_B4_FFT.csv');
import_fft_B4_P3=uiimport('C:\Users\Public\Documents\Dewesoft\Ex
ports\D0\FFTs\D0_P3_B4_FFT.csv');
import_fft_B4_P4=uiimport('C:\Users\Public\Documents\Dewesoft\Ex
ports\D0\FFTs\D0_P4_B4_FFT.csv');

% Barrido 5
import_fft_B5_P1=uiimport('C:\Users\Public\Documents\Dewesoft\Ex
ports\D0\FFTs\D0_P1_B5_FFT.csv');
import_fft_B5_P2=uiimport('C:\Users\Public\Documents\Dewesoft\Ex
ports\D0\FFTs\D0_P2_B5_FFT.csv');
import_fft_B5_P3=uiimport('C:\Users\Public\Documents\Dewesoft\Ex
ports\D0\FFTs\D0_P3_B5_FFT.csv');
```

```
import_fft_B5_P4=uiimport('C:\Users\Public\Documents\Dewesoft\Exports\D0\FFTs\D0_P4_B5_FFT.csv');


% ORDENACIÓN DE LOS DATOS

% Barrido 1
B1_P1_fft_data=import_fft_B1_P1.data;
B1_P1_fft_data_nan=isnan(B1_P1_fft_data); % Comprueba si hay celdas erroneas
find(B1_P1_fft_data_nan==1); % señala las celdas erroneas
B1_P1_fft_data(:,end)=[]; % borra los ultimos valores de frecuencia, A1 y A2 que parecen ser erroneos
B1_P1_fft_freq=B1_P1_fft_data(1,:);
B1_P1_fft_A1=B1_P1_fft_data(2,:);
B1_P1_fft_A2=B1_P1_fft_data(3,:);

B1_P2_fft_data=import_fft_B1_P2.data;
B1_P2_fft_data_nan=isnan(B1_P2_fft_data);
find(B1_P2_fft_data_nan==1);
B1_P2_fft_data(:,end)=[];
B1_P2_fft_freq=B1_P2_fft_data(1,:);
B1_P2_fft_A1=B1_P2_fft_data(2,:);
B1_P2_fft_A2=B1_P2_fft_data(3,:);

B1_P3_fft_data=import_fft_B1_P3.data;
B1_P3_fft_data_nan=isnan(B1_P3_fft_data);
find(B1_P3_fft_data_nan==1);
B1_P3_fft_data(:,end)=[];
B1_P3_fft_freq=B1_P3_fft_data(1,:);
B1_P3_fft_A1=B1_P3_fft_data(2,:);
B1_P3_fft_A2=B1_P3_fft_data(3,:);

B1_P4_fft_data=import_fft_B1_P4.data;
B1_P4_fft_data_nan=isnan(B1_P4_fft_data);
find(B1_P4_fft_data_nan==1);
B1_P4_fft_data(:,end)=[];
B1_P4_fft_freq=B1_P4_fft_data(1,:);
B1_P4_fft_A1=B1_P4_fft_data(2,:);
B1_P4_fft_A2=B1_P4_fft_data(3,:);

% Barrido 2
B2_P1_fft_data=import_fft_B2_P1.data;
B2_P1_fft_data_nan=isnan(B2_P1_fft_data);
find(B2_P1_fft_data_nan==1);
B2_P1_fft_data(:,end)=[];
B2_P1_fft_freq=B2_P1_fft_data(1,:);
B2_P1_fft_A1=B2_P1_fft_data(2,:);
B2_P1_fft_A2=B2_P1_fft_data(3,:);

B2_P2_fft_data=import_fft_B2_P2.data;
B2_P2_fft_data_nan=isnan(B2_P2_fft_data);
```

```
find(B2_P2_fft_data_nan==1);
B2_P2_fft_data(:,end)=[];
B2_P2_fft_freq=B2_P2_fft_data(1,:);
B2_P2_fft_A1=B2_P2_fft_data(2,:);
B2_P2_fft_A2=B2_P2_fft_data(3,:);

B2_P3_fft_data=import_fft_B2_P3.data;
B2_P3_fft_data_nan=isnan(B2_P3_fft_data);
find(B2_P3_fft_data_nan==1);
B2_P3_fft_data(:,end)=[];
B2_P3_fft_freq=B2_P3_fft_data(1,:);
B2_P3_fft_A1=B2_P3_fft_data(2,:);
B2_P3_fft_A2=B2_P3_fft_data(3,:);

B2_P4_fft_data=import_fft_B2_P4.data;
B2_P4_fft_data_nan=isnan(B2_P4_fft_data);
find(B2_P4_fft_data_nan==1);
B2_P4_fft_data(:,end)=[];
B2_P4_fft_freq=B2_P4_fft_data(1,:);
B2_P4_fft_A1=B2_P4_fft_data(2,:);
B2_P4_fft_A2=B2_P4_fft_data(3,:);


% Barrido 3
B3_P1_fft_data=import_fft_B3_P1.data;
B3_P1_fft_data_nan=isnan(B3_P1_fft_data);
find(B3_P1_fft_data_nan==1);
B3_P1_fft_data(:,end)=[];
B3_P1_fft_freq=B3_P1_fft_data(1,:);
B3_P1_fft_A1=B3_P1_fft_data(2,:);
B3_P1_fft_A2=B3_P1_fft_data(3,:);

B3_P2_fft_data=import_fft_B3_P2.data;
B3_P2_fft_data_nan=isnan(B3_P2_fft_data);
find(B3_P2_fft_data_nan==1);
B3_P2_fft_data(:,end)=[];
B3_P2_fft_freq=B3_P2_fft_data(1,:);
B3_P2_fft_A1=B3_P2_fft_data(2,:);
B3_P2_fft_A2=B3_P2_fft_data(3,:);

B3_P3_fft_data=import_fft_B3_P3.data;
B3_P3_fft_data_nan=isnan(B3_P3_fft_data);
find(B3_P3_fft_data_nan==1);
B3_P3_fft_data(:,end)=[];
B3_P3_fft_freq=B3_P3_fft_data(1,:);
B3_P3_fft_A1=B3_P3_fft_data(2,:);
B3_P3_fft_A2=B3_P3_fft_data(3,:);

B3_P4_fft_data=import_fft_B3_P4.data;
B3_P4_fft_data_nan=isnan(B3_P4_fft_data);
find(B3_P4_fft_data_nan==1);
B3_P4_fft_data(:,end)=[];
B3_P4_fft_freq=B3_P4_fft_data(1,:);
```

```
B3_P4_fft_A1=B3_P4_fft_data(2,:);
B3_P4_fft_A2=B3_P4_fft_data(3,:);

% Barrido 4
B4_P1_fft_data=import_fft_B4_P1.data;
B4_P1_fft_data_nan=isnan(B4_P1_fft_data);
find(B4_P1_fft_data_nan==1);
B4_P1_fft_data(:,end)=[];
B4_P1_fft_freq=B4_P1_fft_data(1,:);
B4_P1_fft_A1=B4_P1_fft_data(2,:);
B4_P1_fft_A2=B4_P1_fft_data(3,:);

B4_P2_fft_data=import_fft_B4_P2.data;
B4_P2_fft_data_nan=isnan(B4_P2_fft_data);
find(B4_P2_fft_data_nan==1);
B4_P2_fft_data(:,end)=[];
B4_P2_fft_freq=B4_P2_fft_data(1,:);
B4_P2_fft_A1=B4_P2_fft_data(2,:);
B4_P2_fft_A2=B4_P2_fft_data(3,:);

B4_P3_fft_data=import_fft_B4_P3.data;
B4_P3_fft_data_nan=isnan(B4_P3_fft_data);
find(B4_P3_fft_data_nan==1);
B4_P3_fft_data(:,end)=[];
B4_P3_fft_freq=B4_P3_fft_data(1,:);
B4_P3_fft_A1=B4_P3_fft_data(2,:);
B4_P3_fft_A2=B4_P3_fft_data(3,:);

B4_P4_fft_data=import_fft_B4_P4.data;
B4_P4_fft_data_nan=isnan(B4_P4_fft_data);
find(B4_P4_fft_data_nan==1);
B4_P4_fft_data(:,end)=[];
B4_P4_fft_freq=B4_P4_fft_data(1,:);
B4_P4_fft_A1=B4_P4_fft_data(2,:);
B4_P4_fft_A2=B4_P4_fft_data(3,:);

% Barrido 5
B5_P1_fft_data=import_fft_B5_P1.data;
B5_P1_fft_data_nan=isnan(B5_P1_fft_data);
find(B5_P1_fft_data_nan==1);
B5_P1_fft_data(:,end)=[];
B5_P1_fft_freq=B5_P1_fft_data(1,:);
B5_P1_fft_A1=B5_P1_fft_data(2,:);
B5_P1_fft_A2=B5_P1_fft_data(3,:);

B5_P2_fft_data=import_fft_B5_P2.data;
B5_P2_fft_data_nan=isnan(B5_P2_fft_data);
find(B5_P2_fft_data_nan==1);
B5_P2_fft_data(:,end)=[];
B5_P2_fft_freq=B5_P2_fft_data(1,:);
B5_P2_fft_A1=B5_P2_fft_data(2,:);
B5_P2_fft_A2=B5_P2_fft_data(3,:);
```

```
B5_P3_fft_data=import_fft_B5_P3.data;
B5_P3_fft_data_nan=isnan(B5_P3_fft_data);
find(B5_P3_fft_data_nan==1);
B5_P3_fft_data(:,end)=[];
B5_P3_fft_freq=B5_P3_fft_data(1,:);
B5_P3_fft_A1=B5_P3_fft_data(2,:);
B5_P3_fft_A2=B5_P3_fft_data(3,:);

B5_P4_fft_data=import_fft_B5_P4.data;
B5_P4_fft_data_nan=isnan(B5_P4_fft_data);
find(B5_P4_fft_data_nan==1);
B5_P4_fft_data(:,end)=[];
B5_P4_fft_freq=B5_P4_fft_data(1,:);
B5_P4_fft_A1=B5_P4_fft_data(2,:);
B5_P4_fft_A2=B5_P4_fft_data(3,:);



% PROMEDIADO

% Barrido 1
Pmean_fft_B1_A1=mean([B1_P1_fft_A1;B1_P2_fft_A1;B1_P3_fft_A1;B1_
P4_fft_A1]);
Pmean_fft_B1_A2=mean([B1_P1_fft_A2;B1_P2_fft_A2;B1_P3_fft_A2;B1_
P4_fft_A2]);

% Barrido 2
Pmean_fft_B2_A1=mean([B2_P1_fft_A1;B2_P2_fft_A1;B2_P3_fft_A1;B2_
P4_fft_A1]);
Pmean_fft_B2_A2=mean([B2_P1_fft_A2;B2_P2_fft_A2;B2_P3_fft_A2;B2_
P4_fft_A2]);

% Barrido 3
Pmean_fft_B3_A1=mean([B3_P1_fft_A1;B3_P2_fft_A1;B3_P3_fft_A1;B3_
P4_fft_A1]);
Pmean_fft_B3_A2=mean([B3_P1_fft_A2;B3_P2_fft_A2;B3_P3_fft_A2;B3_
P4_fft_A2]);

% Barrido 4
Pmean_fft_B4_A1=mean([B4_P1_fft_A1;B4_P2_fft_A1;B4_P3_fft_A1;B4_
P4_fft_A1]);
Pmean_fft_B4_A2=mean([B4_P1_fft_A2;B4_P2_fft_A2;B4_P3_fft_A2;B4_
P4_fft_A2]);

% Barrido 5
Pmean_fft_B5_A1=mean([B5_P1_fft_A1;B5_P2_fft_A1;B5_P3_fft_A1;B5_
P4_fft_A1]);
Pmean_fft_B5_A2=mean([B5_P1_fft_A2;B5_P2_fft_A2;B5_P3_fft_A2;B5_
P4_fft_A2]);
```

```
% SOLAPAMIENTO DE LAS FFT

% Borramos las frecuencias de cada barrido fuera de la region de
interes
Pmean_fft_B1_A1(10e3:30e3)=0;
Pmean_fft_B2_A1([1:5000,15e3:30e3])=0;
Pmean_fft_B3_A1([1:10e3,20e3:30e3])=0;
Pmean_fft_B4_A1([1:15e3,25e3:30e3])=0;
Pmean_fft_B5_A1(1:20e3)=0;
% Sumamos todos los barridos, se solapan en toda la region menos
en los extremos
Pmean_fft_BX_A1=Pmean_fft_B1_A1+Pmean_fft_B2_A1+Pmean_fft_B3_A1+
Pmean_fft_B4_A1+Pmean_fft_B5_A1;
% Hacemos la media de los valores en la region central donde
hubo solapamiento
Pmean_fft_BX_A1(5000:25000)=Pmean_fft_BX_A1(5000:25000)/2;

% Repetimos con A2
Pmean_fft_B1_A2(10e3:30e3)=0;
Pmean_fft_B2_A2([1:5000,15e3:30e3])=0;
Pmean_fft_B3_A2([1:10e3,20e3:30e3])=0;
Pmean_fft_B4_A2([1:15e3,25e3:30e3])=0;
Pmean_fft_B5_A2(1:20e3)=0;
Pmean_fft_BX_A2=Pmean_fft_B1_A2+Pmean_fft_B2_A2+Pmean_fft_B3_A2+
Pmean_fft_B4_A2+Pmean_fft_B5_A2;
Pmean_fft_BX_A2(5000:25000)=Pmean_fft_BX_A2(5000:25000)/2;


% Pasamos las graficas finales por una media movil para
suavizarlas
Pmean_fft_BX_A1_smoothed_D0=mediamovil(Pmean_fft_BX_A1,25);
Pmean_fft_BX_A2_smoothed_D0=mediamovil(Pmean_fft_BX_A2,25);


% close all

figure
handle=gca
handle.XAxis.Exponent=0
hold on
plot(B1_P1_fft_freq,Pmean_fft_BX_A1_smoothed_D0)
plot(B1_P1_fft_freq,Pmean_fft_BX_A2_smoothed_D0)
ylabel('A [m/s^2]')
xlabel('Frequency [Hz]')
xlim([0,30e3])
grid on
grid minor
legend('RW','DW')
title('FFT-D0')
```

1.2.2 Moving average

```
%{
FUNCION PARA LA MEDIA MOVIL

ENRTRADAS
     input: vector con los datos a los que se les hace la media
     movil
     N: numero de puntos que se toman a izquierda y derecha para
     la media móvil

SALIDA
    out: vector con la media móvil de la entrada
%}

function out = mediamovil (input,N)
meanrange=zeros(length(input),1);

for index=1:length(input)
    lowrange=max(index-N,1);
    highrange=min(index+N,length(input));
    range=[lowrange:highrange];
    meanrange(index)=mean(input(range));
end

out=meanrange;
```

1.3 Transmissibility

```
% TRANSMISIBILIDAD

transmisibilidad_D0_A_dB=20*log10(Pmean_fft_BX_A1_smoothed_D0./P
mean_fft_BX_A1_smoothed_D0);

transmisibilidad_DS_A1_dB=20*log10(Pmean_fft_BX_A1_smoothed_DS./
Pmean_fft_BX_A1_smoothed_D0);
transmisibilidad_DS_A2_dB=20*log10(Pmean_fft_BX_A2_smoothed_DS./
Pmean_fft_BX_A2_smoothed_D0);

transmisibilidad_DL_A1_dB=20*log10(Pmean_fft_BX_A1_smoothed_DL./
Pmean_fft_BX_A1_smoothed_D0);
transmisibilidad_DL_A2_dB=20*log10(Pmean_fft_BX_A2_smoothed_DL./
Pmean_fft_BX_A2_smoothed_D0);

transmisibilidad_DSL_A1_dB=20*log10(Pmean_fft_BX_A1_smoothed_DSL
./Pmean_fft_BX_A1_smoothed_D0);
transmisibilidad_DSL_A2_dB=20*log10(Pmean_fft_BX_A2_smoothed_DSL
./Pmean_fft_BX_A2_smoothed_D0);


figure
handle=gca
handle.XAxis.Exponent=0
hold on
plot(B1_P1_fft_freq,transmisibilidad_DS_A1_dB)
plot(B1_P1_fft_freq,transmisibilidad_DS_A2_dB)
plot(B1_P1_fft_freq,transmisibilidad_D0_A_dB)
ylabel('Transmissibility [dB]')
xlabel('Frequency [Hz]')
xlim([0,30e3])
grid on
grid minor
legend('RW','DW','D0')
title('Transmissibility DS-D0')


figure
handle=gca
handle.XAxis.Exponent=0
hold on
plot(B1_P1_fft_freq,transmisibilidad_DL_A1_dB)
plot(B1_P1_fft_freq,transmisibilidad_DL_A2_dB)
plot(B1_P1_fft_freq,transmisibilidad_D0_A_dB)
ylabel('Transmissibility [dB]')
xlabel('Frequency [Hz]')
xlim([0,30e3])
grid on
grid minor
legend('RW','DW','D0')
```

```
title('Transmissibility DL-D0')

figure
handle=gca
handle.XAxis.Exponent=0
hold on
plot(B1_P1_fft_freq,transmisibilidad_DSL_A1_dB)
plot(B1_P1_fft_freq,transmisibilidad_DSL_A2_dB)
plot(B1_P1_fft_freq,transmisibilidad_D0_A_dB)
ylabel('Transmissibility [dB]')
xlabel('Frequency [Hz]')
xlim([0,30e3])
grid on
grid minor
legend('RW','DW','D0')
title('Transmissibility DSL-D0')


figure
handle=gca
handle.XAxis.Exponent=0
hold on
plot(B1_P1_fft_freq,transmisibilidad_DS_A1_dB)
plot(B1_P1_fft_freq,transmisibilidad_DL_A1_dB)
plot(B1_P1_fft_freq,transmisibilidad_DSL_A1_dB)
yline(0)
ylabel('Transmissibility [dB]')
xlabel('Frequency [Hz]')
xlim([0,30e3])
grid on
grid minor
legend('DS','DL','DSL')
title('Transmissibility RW')


figure
handle=gca
handle.XAxis.Exponent=0
hold on
plot(B1_P1_fft_freq,transmisibilidad_DS_A2_dB)
plot(B1_P1_fft_freq,transmisibilidad_DL_A2_dB)
plot(B1_P1_fft_freq,transmisibilidad_DSL_A2_dB)
yline(0)
ylabel('Transmissibility [dB]')
xlabel('Frequency [Hz]')
xlim([0,30e3])
grid on
grid minor
legend('DS','DL','DSL')
title('Transmissibility DW')
```

```
figure
handle=gca
handle.XAxis.Exponent=0
hold on
plot(B1_P1_fft_freq,Pmean_fft_BX_A1_smoothed_D0)
plot(B1_P1_fft_freq,Pmean_fft_BX_A1_smoothed_DS)
plot(B1_P1_fft_freq,Pmean_fft_BX_A1_smoothed_DL)
plot(B1_P1_fft_freq,Pmean_fft_BX_A1_smoothed_DSL)
yline(0)
ylabel('A [m/s^2]')
xlabel('Frequency [Hz]')
xlim([0,30e3])
grid on
grid minor
legend('D0','DS','DL','DSL')
title('FFT-RW')


figure
handle=gca
handle.XAxis.Exponent=0
hold on
plot(B1_P1_fft_freq,Pmean_fft_BX_A2_smoothed_D0)
plot(B1_P1_fft_freq,Pmean_fft_BX_A2_smoothed_DS)
plot(B1_P1_fft_freq,Pmean_fft_BX_A2_smoothed_DL)
plot(B1_P1_fft_freq,Pmean_fft_BX_A2_smoothed_DSL)
yline(0)
ylabel('A [m/s^2]')
xlabel('Frequency [Hz]')
xlim([0,30e3])
grid on
grid minor
legend('D0','DS','DL','DSL')
title('FFT-DW')
```